Geoscience Frontiers 12 (2021) 101243

Contents lists available at ScienceDirect

Geoscience Frontiers

journal homepage: www.elsevier.com/locate/gsf

Research Paper

Petrogenesis and tectonic implications of the Triassic rhyolites in the East Kunlun Orogenic Belt, northern Tibetan Plateau

Fengli Shao [a,b,*], Yaoling Niu [b,c,d], Juanjuan Kong [e], Yi Liu [f], Guodong Wang [g], Yu Zhang [b]

[a] Institute of Geology and Paleontology, Linyi University, Linyi 276000, China
[b] Laboratory for Marine Geology, Qingdao National Laboratory for Marine Science and Technology, Qingdao 266061, China
[c] Department of Earth Sciences, Durham University, Durham DH1 3LE, UK
[d] School of Earth Science and Resources, China University of Geosciences, Beijing 100083, China
[e] College of Ocean Science and Engineering, Shandong University of Science and Technology, Qingdao 266590, China
[f] Faculty of Land Resources Engineering, Kunming University of Science and Technology, Kunming 650093, China
[g] School of Resources and Environment, Linyi University, Linyi 276000, China

ARTICLE INFO

Article history:
Received 1 January 2021
Revised 14 May 2021
Accepted 27 May 2021
Available online 29 May 2021

Handling Editor: W.J. Xiao

Keywords:
East Kunlun
Tibetan Plateau
Peralkaline rhyolites
Elashan formation

ABSTRACT

The East Kunlun Orogenic Belt (EKOB), which is in the northern part of the Greater Tibetan Plateau, contains voluminous Late Triassic intermediate-felsic volcanic rocks. In the east end of the EKOB, we identified highly differentiated peralkaline-like Xiangride rhyolites (~209 Ma) that differ from the widespread andesitic-rhyolitic Elashan volcanics (~232–225 Ma) in terms of their field occurrences and mineral assemblages. The older, more common calc-alkaline felsic Elashan volcanics may have originated from partial melting of the underthrust Paleo-Tethys oceanic crust under amphibolite facies conditions associated with continental collision. The felsic Elashan volcanics and *syn*-collisional granitoids of the EKOB are different products of the same magmatic event related to continental collision. The Xiangride rhyolites are characterized by elevated abundances of high field strength elements, especially the very high Nb and Ta contents, the very low Ba, Sr, Eu, P, and Ti contents; and the variably high $^{87}Sr/^{86}Sr$ ratios (up to 0.96), exhibiting remarkable similarities to the characteristic peralkaline rhyolites. The primitive magmas parental to the Xiangride rhyolites were most likely alkali basaltic magmas that underwent protracted fractional crystallization with continental crust contamination. The rock associations from the early granitoids and calc-alkaline volcanic rocks to the late alkaline basaltic dikes and peralkaline-like rhyolites in the Triassic provide important information about the tectonic evolution of the EKOB from *syn*-collisional to post-collisional. We infer that the transition from collisional compression to post-collisional extension occurred at about 220 Ma.

1. Introduction

The East Kunlun Orogenic belt (EKOB), located in the northern part of the Greater Tibetan Plateau, is a giant tectono-magmatic belt that is comparable to the Gangdese belt to the south (Fig. 1a) (Mo et al., 2007). With the Altyn fault to the west and the Wenquan fault to the east, the EKOB stretches for about 1500 km and exhibits N–S extension for 50–200 km. The Paleoproterozoic Jinshuikou Group (~2.39 Ga; high-amphibolite and granulite facies metamorphic rock series; Gong et al., 2012; Li et al., 2021) and the Mesoproterozoic Kuhai Complex are considered to be the basement rocks of the EKOB (Liu et al., 2016). As a compound orogeny, the EKOB preserves the overprinted geological records of the Early Paleozoic Caledonian cycles and the Late Paleozoic to Early Mesozoic Variscan-Indosinian cycle. Significantly, the petrotectonic assemblages of the East Kunlun Caledonian cycle are comparable to those in the North Qilian orogenic belt, and the integral Variscan-Indosinian cycle resembles the Paleo-Tethys evolutionary history in the Sanjiang area, southwestern China (Liu et al., 2013; Huang et al., 2015, 2016; Wang et al., 2018; 2019;; Li et al., 2020; Xu et al., 2020b).

The abundant Late Paleozoic to Early Mesozoic igneous rocks provided a good record of the long-term tectonic evolution and orogenesis of the EKOB (Chen et al., 2019b; Dong et al., 2018; Li et al., 2012; Xu et al., 2007). Significant volumes of Permian-Triassic granitoid plutons and volcanic rocks outcrop throughout

* Corresponding author at: Institute of Geology and Paleontology, Linyi University, Middle Part of Shuangling Road, Lanshan District, Linyi 276000, China.
E-mail address: fenglishao@126.com (F. Shao).

https://doi.org/10.1016/j.gsf.2021.101243
1674-9871/

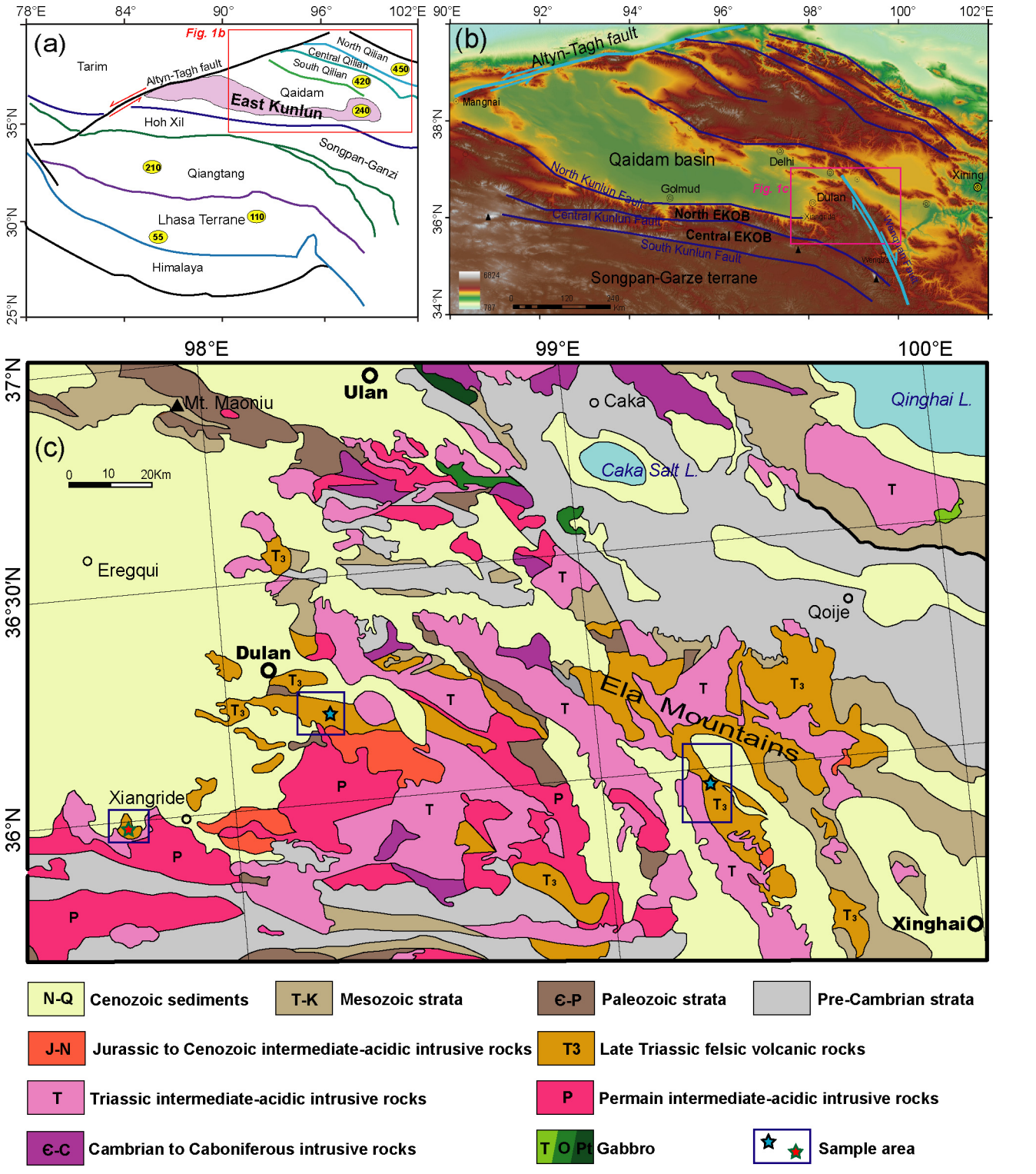

Fig. 1. (a) Tectonic framework of the Greater Tibetan Plateau (after Mo et al., 2008; Niu et al., 2013). The numbers in the yellow ellipse represent ages of magmatic rocks in these orogenic belts. (b) Topographic image showing the sub-tectonic units of the East Kunlun Orogenic belt (EKOB) (after Shao et al., 2017). (c) Simplified geological map of the eastern part of the EKOB (modified from 1:1,000,000, Geological Map by the Chinese Geological Survey). The boxes with stars indicate sample locations in this study with sample details given in Supplementary data Table S1.

the EKOB (Fig. 1c). The intrusive rocks are dominated by granites and granodiorites containing abundant mafic magmatic enclaves (Huang et al., 2014; Xia et al., 2014, 2015; Shao et al., 2017). The Late Triassic volcanic rocks belong to the Elashan Formation and the Babaoshan Formation (Xiong et al., 2014; Li et al., 2015a; Hu et al., 2016; Ren et al., 2016; Xu et al., 2020a). The EKOB formed in the Paleo-Tethys related Wilson cycle during the Late Paleozoic to Early Mesozoic and records the history of the Anyemaqen Ocean, which was a branch of the Paleo-Tethys Ocean (Jiang et al., 1992; Yang et al., 1996). The timing of the seafloor subduction (Yang et al., 1996, 2009; Liu et al., 2011; Dong et al., 2018), ocean closing (Yan et al., 2008; Li et al., 2012), and continental collision (Chen

et al., 2019a,b; Guo et al., 1998; Liu et al., 2015) remain controversial. For example, Yang et al (2009) inferred that the Anyemaqen Ocean opened in the Late Carboniferous (308 ± 4.9 Ma) based on the Dur'ngio ophiolite; while Liu et al. (2011) argued for an Early Carboniferous opening (332.8 ± 3.1 Ma). Luo et al (2014) concluded that the transition from subduction to collision took place in the Late Triassic, while others concluded the onset of collision occurred in the Middle Triassic (Xia et al., 2014) or even the Early Triassic (Yang et al., 2009). The tectonic evolution of the EKOB is important to gaining a better understanding of the amalgamation of the Greater Tibetan Plateau.

Ding et al. (2011) identified a suite of high Nb-Ta rhyolites whose characteristics differ from the widespread Elashan rhyolites, but have been mistaken for the Triassic Elashan Formation (Bureau of geological exploration and development of Qinghai Province, 1991). Compared with the Elashan rhyolites, the high Nb-Ta rhyolites have high SiO_2 and K_2O contents, high peralkaline index values (i.e., *P.I.* = molar $[Na_2O + K_2O]/Al_2O_3$), low Al_2O_3 and CaO contents, and are enriched in high field strength elements (HFSEs) (e.g., Nb, Ta, and Zr), resembling the typical peralkaline rhyolites in eastern Australia (Glass House Mountains; Shao et al., 2015) and northeastern China (Changbaishan, unpublished data). Two contrasting models have been proposed for the origin of these peralkaline rhyolites: (i) the production of low-volume end products as a result of protracted fractional crystallization from transitional to alkali basaltic magmas (Kar et al., 1998; Peccerillo et al., 2003, 2007; Mbassa et al., 2012; White et al., 2012; Hutchison et al., 2016; Chandler and Spandler, 2020); and (ii) partial melting of continental crust or a mafic intrusive body (Lowenstern and Mahood, 1991; Black et al., 1997; Bohrson and Reid, 1997; Renna et al., 2013). The compositional and age differences between the older calc-alkaline Elashan rhyolites (~232–225 Ma) and the younger peralkaline-like high Nb-Ta rhyolites (~209 Ma) indicate that they are the products of different magmatic events. Through the comparative analysis of new high-quality data, we investigated the petrogenesis of the Elashan rhyolites and the peralkaline-like rhyolites. These two compositionally distinctive suites of rhyolites with an age difference of ~15 Myr are ideal for discussing the tectonic evolution of the EKOB.

In this paper, we use U-Pb zircon ages, bulk-rock major and trace element compositions, and Sr-Nd-Pb-Hf isotope data to discuss the petrogenesis of these two suites of Late Triassic rhyolites and their associated andesites and dacites in the context of the tectonic evolution of the EKOB.

2. Geology and samples

The Late Triassic Elashan Formation is dominated by pyroclastic rocks, with intercalated lavas and unstable sedimentary clastic rock layers (Ding et al., 2011). The volcanism recorded in the Elashan Formation was produced by a central continental eruption with a large eruption intensity and extensive distribution (Lu et al., 2012; Li and Liu, 2014; Li et al., 2015a; Ma et al., 2016). The volcanic rocks of the Elashan Formation (235–212 Ma), which vary upwards from intermediate-mafic to intermediate-felsic, are widely distributed in the EKOB (Ni, 2010; Qi, 2015). Remarkably, the high Nb-Ta rhyolites only outcrop near the Xiangride town, with no contemporary mafic and intermediate volcanic rocks.

We collected 21 representative samples (Supplementary data Table S1) from the eastern end of the EKOB, including rhyolites, dacites, andesites, and basalts from the Elashan Formation in the Elashan area (i.e., Elashan volcanic rocks in the figures) and peralkaline-like high Nb-Ta rhyolites near Xiangride town (Xiangride rhyolites). The Xiangride rhyolites display complete volcanic necks, columnar joints of varying diameters (~20–50 cm), and flow structures that can be seen on the hand specimen scale (Fig. 2a–c). The fresh rocks are reddish-brown and have a porphyritic texture and massive or fluidal structures. The phenocrysts are mainly quartz, orthoclase, and minor plagioclase. The aphanitic matrix exhibits a fluidal structure and vesicles filled with acicular silicates, subhedral quartz, and feldspar. The Elashan volcanic rocks are mainly purplish-red and greyish-green rhyolitic ignimbrite and minor dacite and andesite. The pyroclasts are both crystal clasts (plagioclases and quarts, 1–2 mm) and vitroclasts (2–3 mm) in the aphanitic matrix. Secondary minerals such as chlorite, epidote and sericite occur in the altered samples.

3. Analytical methods

We cut all of the specimens into ~1 cm thick slab to remove the effects of weathering and markers and then broke them into 1–2 cm fragments using a percussion mill. Then, the fragments were crushed into smaller pieces using a crusher. In order to analyze the whole rock matrix, which approximates the melt compositions, we pick out only clean chips of matrix of varying size (60–80 mesh) under the binocular microscope. Before the analyses, the selected chips were ultrasonically cleaned in Milli-Q water and were dried in a clean environment.

3.1. U-Pb zircon dating and bulk-rock major and trace element analyses

We observed the morphology and internal structures of the zircons using reflected-light and cathodoluminescence (CL) images. The CL images were captured using the field emission scanning electron microscope (TESCAN-MIRA3) at the Nanjing Hongchuang Exploration Technology Service Co., Ltd. The U-Pb zircon dating and trace element analyses were conducted simultaneously using the 193 nm ArF excimer laser (Photon-Machines) and inductively coupled plasma mass spectrometer (ICP-MS) (Agilent-7900) system at the Institute of Oceanology, Chinese Academy of Science (IOCAS), following the methods reported by Xiao et al. (2020). The off-line data processing and age calculations were conducted using the *ICPMS-DataCal* (Liu et al., 2010) and Isoplot/Ex-ver 4.15 (Ludwig, 2012) softwares. The bulk-rock major element (Agilent-5100 ICP-OES) and trace element (Agilent-7900 ICP-MS) analyses were conducted at the IOCAS, following the methods reported by Kong et al. (2019b) and Chen et al. (2017), respectively. United States geological Survey (USGS) rock standards AGV-2, STM-2, and RGM-2 were analyzed along with the unknown samples to monitor the analytical accuracy (±5%) and precision (<2%; Supplementary data Table S2) of the major element analysis. USGS standards AGV-2, GSP-2, RGM-2, BCR-2, and BHVO-2 were used to monitor the analytical accuracy and precision of the trace element analysis (better than 5% for most elements; Supplementary data Table S3).

3.2. Bulk-rock Sr-Nd-Pb-Hf isotopes

the bulk-rock Sr-Nd-Pb-Hf isotope analysis was conducted at the IOCAS. First, the Sr and Pb were separated using Sr-Spec resin. Then, AG 50 W-X8 resin was used to separate the rare earth elements (REEs) and high field strength elements (HFSEs). The Nd and Hf were separated using specific Ln-(Nd) and Ln-(Hf) resins, respectively. The details of the sample digestion and Sr-Nd-Pb-Hf separation procedure have been reported by Sun et al. (2018). The isotopic ratios were determined using a Nu Plasma II MC-ICP-MS and were corrected for instrumental mass fractionation using $^{86}Sr/^{88}Sr = 0.1194$, $^{146}Nd/^{144}Nd = 0.7219$, $^{203}Tl/^{205}Tl = 0.4189$, and $^{179}Hf/^{177}Hf = 0.7325$. Repeated analysis of Sr standard NBS-

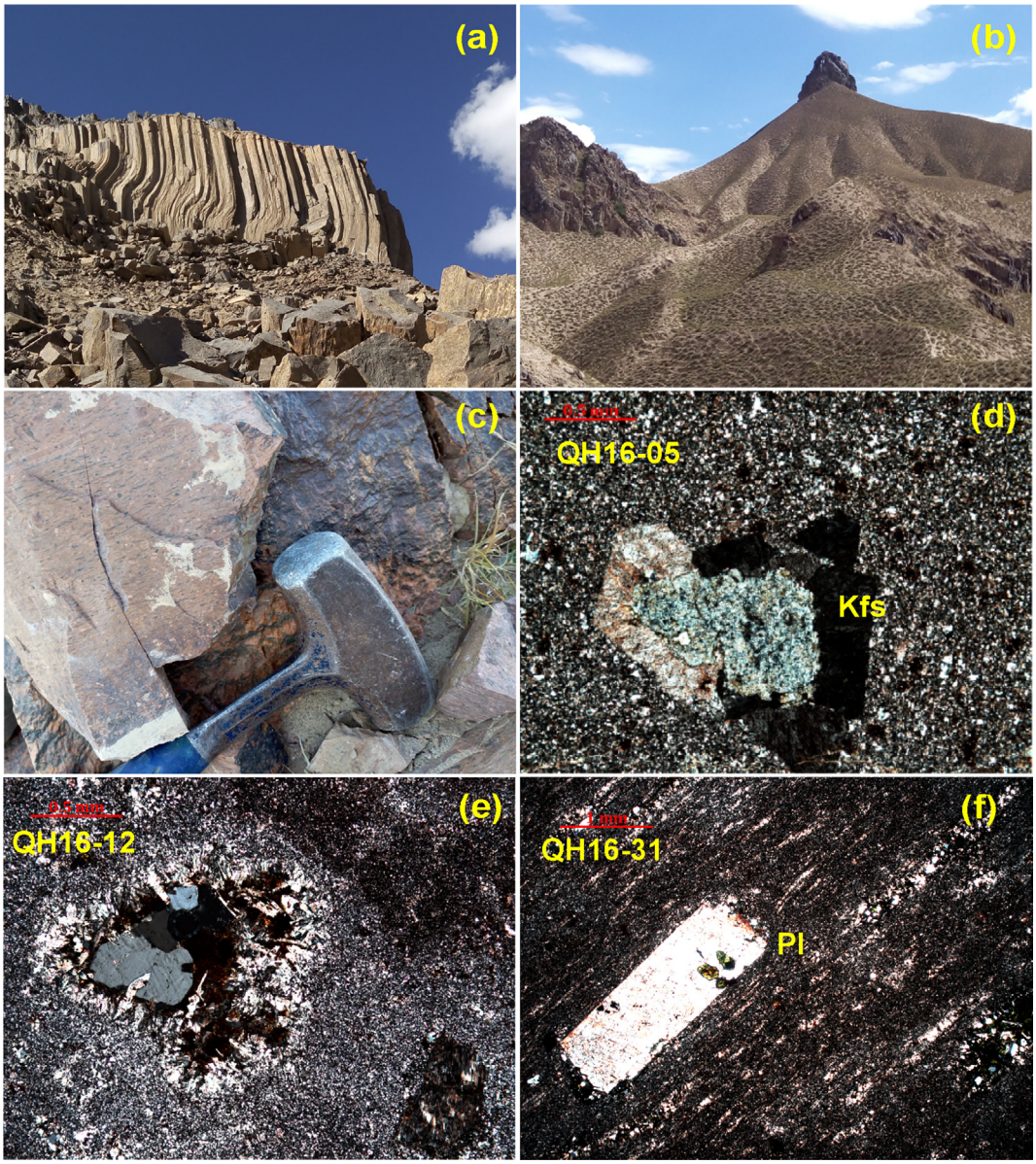

Fig. 2. (a–c) Field occurrence of the rhyolites outcrop near Xiangride Town in the EKOB, exhibiting spectacular columnar joints, intact volcanic neck and typical rhyolitic structure. (d–f) Representative photomicrographs under crossed polarized light, showing orthoclase phenocryst with Carlsbad twin, plagioclase phenocryst and vesicles in the aphanitic matrix with or without flow banding.

987, Nd standard JNdi-1, and Hf standard Alfa-Hf gave $^{87}Sr/^{86}Sr$ = 0.710246 ± 0.000005 (2σ, n = 22), $^{143}Nd/^{144}Nd$ = 0.512102 ± 0.000006 (2σ, n = 11), and $^{176}Hf/^{177}Hf$ = 0.282191 ± 0.000003 (2σ, n = 15), respectively. The mean values for USGS standards AGV-2, GSP-2, and RGM-2 were $^{87}Sr/^{86}Sr$ = 0.704136 ± 0.000005, 0.765534 ± 0.000004, and 0.704726 ± 0.000004 (2σ, n = 3), respectively. Repeated analysis of Pb standard NBS-981 yielded $^{208}Pb/^{204}Pb$ = 36.676 ± 0.001, $^{207}Pb/^{204}Pb$ = 15.489 ± 0.001, and $^{206}Pb/^{204}Pb$ = 16.931 ± 0.001 (2σ, n = 12). The Sr-Nd-Pb-Hf isotopic results of USGS standards AGV-2, GSP-2, and RGM-2 are consistent with the recommended values (Supplementary data Table S4).

4. Results

4.1. U-Pb zircon dating

Most of the zircon grains are colorless and transparent with euhedral to subhedral prismatic or pyramidal shapes. They vary in size (100–300 μm in length, with aspect ratios of 2:1 to 4:1) and exhibit oscillatory and fan-shaped zoning (Fig. 3). The higher the crystallization temperature, the wider the oscillation band because of the faster elemental diffusion (Watson and Harrison, 1983; Pidgeon et al., 1998; Rubatto and Gebauer, 2000). The fan-shaped zoning was caused by the change in the crystallization environment, which resulted in the inconsistent growth rates of the different crystal planes (Vavra et al., 1996). Some of the zircons exhibit different rim and core morphologies, suggesting that the cores may have been inherited or captured (Wu and Zheng, 2004).

We dated zircons from two peralkaline-like Xiangride rhyolites and from an andesite and a rhyolitic ignimbrite from the Elashan volcanic rocks (Fig. 3 and Supplementary data Table S5). The Xiangride rhyolites yielded concordia ages of 208.4 ± 1.6 Ma (QH16-19) and 209.1 ± 0.7 Ma (QH16-31), which are identical within error. The ages of the andesite (QH16-38, 224.6 ± 0.6 Ma) and the rhyolitic ignimbrite (QH16-46, 231.9 ± 1.6 Ma) indicate the magmatic

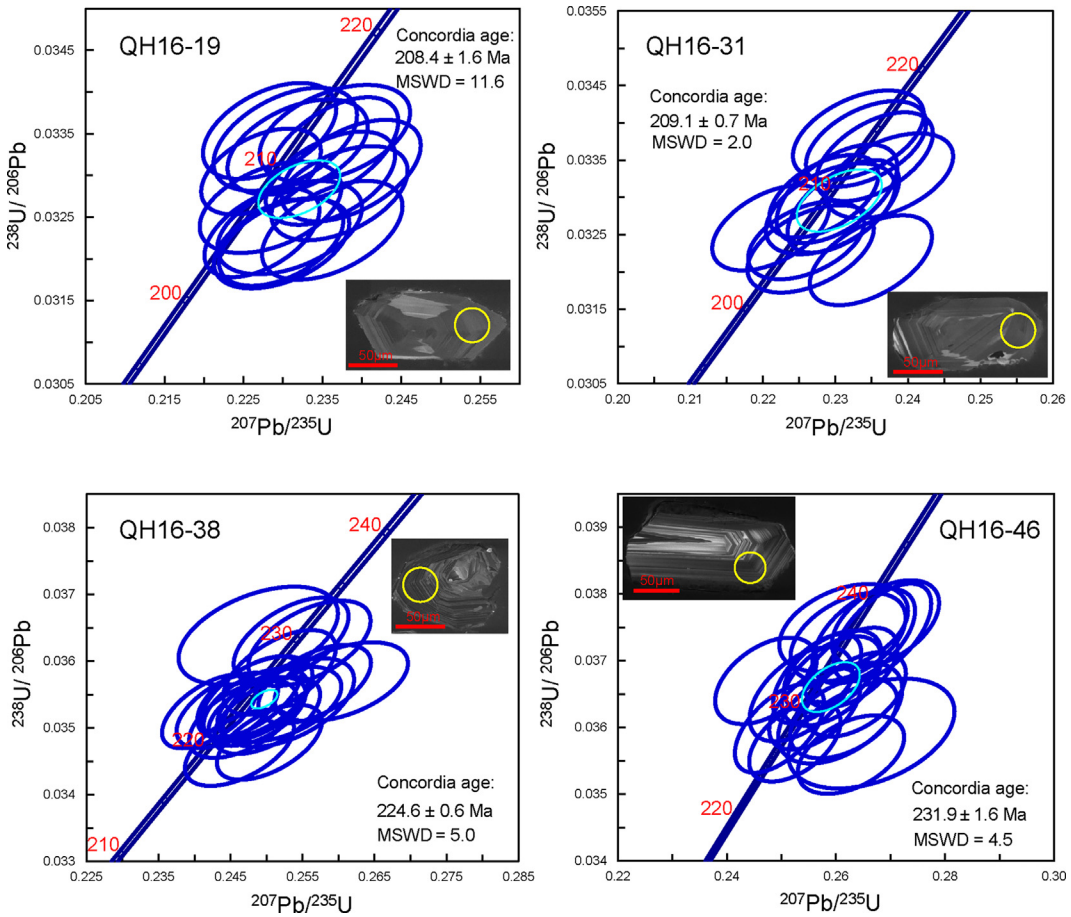

Fig. 3. U-Pb zircon concordia diagrams and cathodoluminescence images of representative zircons for the four dated samples. Yellow circles are the analyzed spots. The U-Pb zircon ages indicate that Xiangride rhyolites are ~15–20 Myr younger than the widespread Elashan rhyolites.

activity of the Elashan Formation started in at least the Middle Triassic.

4.2. Major and trace elements

The Xiangride rhyolites are highly differentiated rhyolites (SiO_2 = 75.10–78.75 wt.%); while the calc-alkaline Elashan volcanic rocks define a compositional spectrum from mafic to felsic (Fig. 4a and Supplementary data Table S6). A series of genetically related rocks from basalts to peralkaline rhyolites in the Glass House Mountains (GHM; Shao et al., 2015) are also plotted for comparison. The peralkaline index of the Xiangride rhyolites (*P.I.* = 0.81–0.96) is similar to that of alkaline A-type granites and peralkaline rhyolites, while the Elashan rhyolites are strongly peraluminous (*P.I.* < 0.80), similar to the abundant *syn*-collisional granites in the EKOB (Fig. 4b) (e.g., Huang et al., 2014; Xia et al., 2014, 2015; Shao et al., 2017). The liquid line of descent (LLD) of the Elashan volcanic rocks (blue solid line) differs significantly from that of the GHM rock series (blue dotted line in Figs. 4, 5); and the total alkali contents of the Elashan volcanic rocks are much lower (and MgO and CaO are significantly higher) than those of the Xiangride and GHM rhyolites at a given silica content.

All of the samples are light rare earth element (LREE) enriched (Fig. 6a). The Xiangride rhyolites have higher rare earth element (REE) content, which are comparable with those of the peralkaline rhyolites from the GHM, Changbaishan (Chen, 2013), and Big Bend National Park (USA; Parker et al., 2012) (Fig. 6b). The Elashan rhyolites exhibit REE patterns similar to that of the bulk continental crust (BCC) but have larger negative Eu anomalies. Compared to the Elashan volcanic rocks, the Xiangride rhyolites have extremely low abundances of Ba, Sr, Eu, P, and Ti contents (Fig. 7 and Supplementary data Table S6). The remarkable negative Ba, Sr, and Eu anomalies ($Eu/Eu^* = [2\times Eu/(Sm + Gd)]_N$ = 0.01–0.02), low CaO and Al_2O_3, and weak peralkalinity of the Xiangride rhyolites indicate significant feldspar (Ca-rich plagioclase and lesser alkaline feldspar) crystallization (Niu and O'Hara, 2009). The P and Ti depletions result from the crystallization of apatite and Ti-rich minerals such as ilmenite and titanomagnetite.

Remarkably, the Xiangride rhyolites have significantly higher Nb and Ta contents than the Elashan volcanic rocks and the upper and bulk continental crust (Fig. 7b) (Rudnick and Gao, 2003) and Nb* and Ta* values (i.e., $Nb^* = [Nb/Th]_{Sample}/[Nb/Th]_{PM}$, $Ta^* = [Ta/U]_{Sample}/[Ta/U]_{PM}$; Niu and Batiza, 1997; Niu et al., 1999) (Fig. 8a) resembling those of mantle derived magmas. The high Nb-Ta contents and Nb/Ta ratios (Fig. 8b) of the Xiangride rhyolites are quite different from those of the EKOB granitoids and felsic Elashan volcanic rocks. Fig. 8a shows that the Elashan rhyolites and the upper continental crust are concentrated in the lower left corner because of their strong Nb and Ta depletion, while the peralkaline rhyolites plot close equal to unity due to their Nb and Ta enrichments. The Xiangride rhyolites plot between the two, which is interpreted to indicate that they are peralkaline rhyolites that have been affected by crustal contamination.

4.3. Bulk-rock Sr-Nd-Pb-Hf isotopes

The Xiangride rhyolites have variably high $^{87}Sr/^{86}Sr$ ratios (0.768896–0.957328). The samples with high $^{87}Sr/^{86}Sr$ ratios have

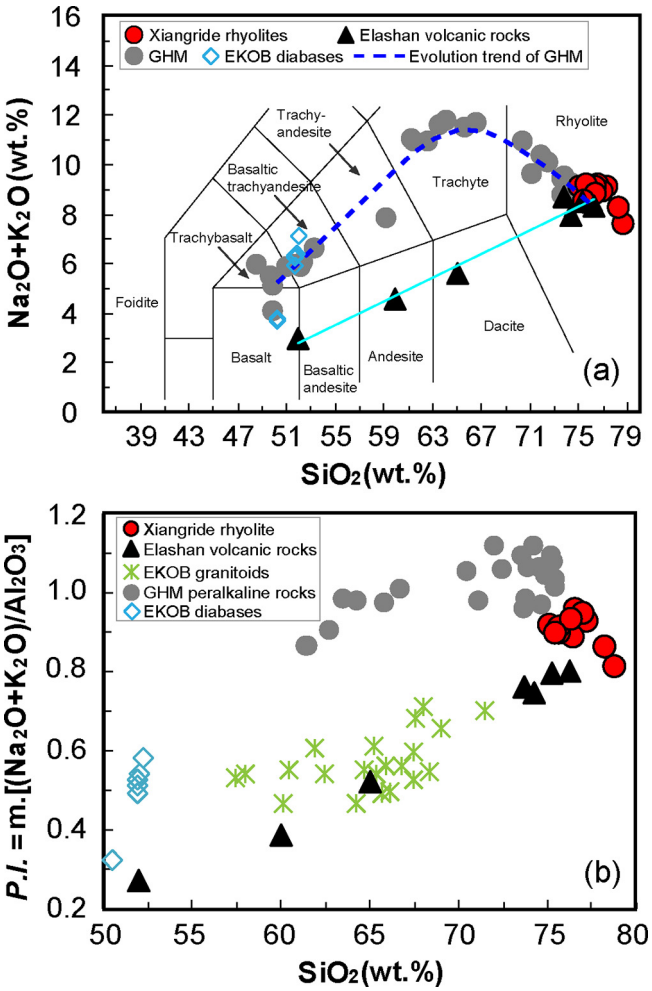

Fig. 4. (a) Total alkalis *vs.* silica diagram to show commotional variation and evolution trend of the Triassic volcanic rocks in the EKOB in comparison with the typical Oligocene alkaline-peralkaline rock association of Glass House Mountains, Australia (GHM, after Shao et al., 2015). (b) Peralkalinity index (*P.I.* = molar [$Na_2O + K_2O$]/Al_2O_3) *vs.* SiO_2. Peraluminous *syn*-collisional granitoids from the EKOB (after Shao et al., 2017), alkaline diabasic dikes from the EKOB (after Hu et al., 2016), and peralkaline trachytes and rhyolites from GHM were plotted for comparation.

extremely low Sr contents (<20 ppm; Fig. 9 and Supplementary data Table S7) and high Rb/Sr ratios. The Sr isotopic signature of the Xiangride rhyolites is the straightforward consequence of Sr depletion (also well as Ba and Eu depletion) due to significant plagioclase (and alkali feldspar to some extent) removal during the protracted fractional crystallization, resembling peralkaline rhyolites (Shao et al., 2015). Thus, the radiogenic ^{87}Sr is largely the result of ^{87}Rb decay after the volcanism occurred. The $^{87}Sr/^{86}Sr$ ratios of the Elashan rocks (except for QH16-39) have restricted values (0.711639–0.726506); while the basalt QH16-39 has a mantle-derived isotopic signature (initial $^{87}Sr/^{86}Sr$ = 0.707841).

The Nd and Hf isotope data for the Xiangride rhyolites essentially have similarly restricted values of $\varepsilon_{Nd}(t)$ (−3.76 to −2.64) and $\varepsilon_{Hf}(t)$ (−1.01 to 1.10, t = 209 Ma; this study; Fig. 10c). The Nd isotope data are consistent with those of Ding et al. (2011). The Elashan volcanic rocks have enriched crustal Nd and Hf isotope values ($\varepsilon_{Nd}(t)$ = −6.72 to −6.10, $\varepsilon_{Hf}(t)$ = −4.16 to −1.11, t = 220 Ma; this study), except for QH16-39 ($\varepsilon_{Nd}(t)$ = −3.79, $\varepsilon_{Hf}(t)$ = 1.63). The Elashan volcanic rocks have a larger range of initial $^{206}Pb/^{204}Pb$ (17.88–18.46) and $^{208}Pb/^{204}Pb$ (35.77–38.36) values than the Xiangride rhyolites ($^{206}Pb/^{204}Pb$ = 18.25–18.43; $^{208}Pb/^{204}Pb$ = 35.96–37.78; Fig. 9d). The initial $^{207}Pb/^{204}Pb$ values (15.58–15.64) of the Elashan volcanic rocks are lower than those of the Xiangride rhyolites (15.64–15.68).

5. Discussion

The field observations and geochemical data presented above demonstrate that there are two distinctive suits of Triassic rhyolites in the EKOB. (i) The Xiangride rhyolites are ~15 Myr younger than the Elashan volcanic rocks. (ii) The Xiangride rhyolites are highly fractionated with high SiO_2 contents and peralkaline index values, and they are characterized by elevated abundances of most incompatible elements, especially very high Nb (*vs.* Th) and Ta (*vs.* U) contents. (iii) The Xiangride rhyolites have variably high $^{87}Sr/^{86}Sr$ ratios. These results provide convincing evidence that the Triassic rhyolites near Xiangride town and in the Elashan area have different origins.

5.1. Origin of the widespread Elashan volcanic rocks

The petrogenesis of the volcanic rocks of the Elashan Formation is controversial. Xu et al. (2019), Xu et al. (2020a) and Tong et al. (2004) concluded that the contemporaneous rhyolites outcropped in the Qimantage area (215 Ma; U-Pb) and the Chachaxiangka area (217 ± 5 Ma; K-Ar) were formed by lower crustal melting in active continental margin and intracontinental orogenic environments, respectively. Li et al. (2015b) argued that the Late Triassic volcanic rocks in the EKOB originated from various depths as a result of lithosphere delamination after continental collision although the mechanism of this delamination is disputed (Sacks and Secor, 1990; Lee and Anderson, 2015). Hu et al. (2016) proposed that the felsic volcanic rocks in the Reshui area (227.5 ± 1.5 Ma; U-Pb) were generated by partial melting of juvenile crustal material due to post-collisional extension and the related orogenic collapse.

The different LLDs and REE contents of the Elashan volcanic rocks and the peralkaline Xiangride rhyolites (Figs. 5, 6) suggest different petrogenetic mechanisms. The variable Ba, Sr, Eu, P, and Ti depletion of the felsic Elashan volcanic rocks indicate that they experienced different degrees of differentiation. Fractional crystallization of the major ore-forming minerals including the pyroxene, amphiboles and feldspar with $D_{Nb} < 1$ and $D_{Ta} < 1$ would increase the Nb, Ta contents in the residual melts. With continuous magmatic differentiation, the Nb/Ta ratios of the felsic Elashan volcanic rocks decreased, resulting in distinctive subchondritic Nb/Ta ratios (5.8–10.4) that are even lower than that of the BCC (11.43; Rudnick and Gao, 2003). Generally, amphibole have $D_{Nb/Ta} > 1$ and fractional crystallization of amphibole from andesitic melts could lead decrease of Nb/Ta ratios and increase of Nb-Ta contents in the residual melts (Adam et al., 1993; Marks et al., 2004). Furthermore, biotite also has $D_{Nb/Ta} > 1$ and fractional crystallization of biotite from rhyolitic melts ($D_{Nb} > 1$ and $D_{Ta} > 1$; Mahood and Hildreth, 1983; Nash and Crecraft, 1985; Ewart and Griffin, 1994) could decrease both the Nb/Ta ratios and the Nb-Ta contents. The combination of lower Nb* and Ta* values (Nb* < 0.1, Ta* ≤ 0.1) and Nb/Ta ratios of the felsic Elashan volcanic rocks illustrates that they cannot be the products of a mantle-derived basaltic magma (Fig. 8). The Elashan volcanic rocks exhibit restricted initial $^{87}Sr/^{86}Sr$ ratios (0.70996 −0.71188) and slightly negative $\varepsilon_{Nd}(t)$ and $\varepsilon_{Hf}(t)$ values. The pre-existing old crustal material beneath the EKOB, which is represented by the lower crustal metamorphic basement composed of the Paleoproterozoic granitic gneiss of the Baishahe Formation (~2.1 Ga; Meng et al., 2005, 2013; Chen et al., 2007; Li et al., 2015a), exhibits high $^{87}Sr/^{86}Sr$ ratios and extremely large negative $\varepsilon_{Nd}(t)$ and $\varepsilon_{Hf}(t)$ values (Shao et al., 2015). Thus, this lower crustal material cannot be the main source of the Elashan volcanic rocks.

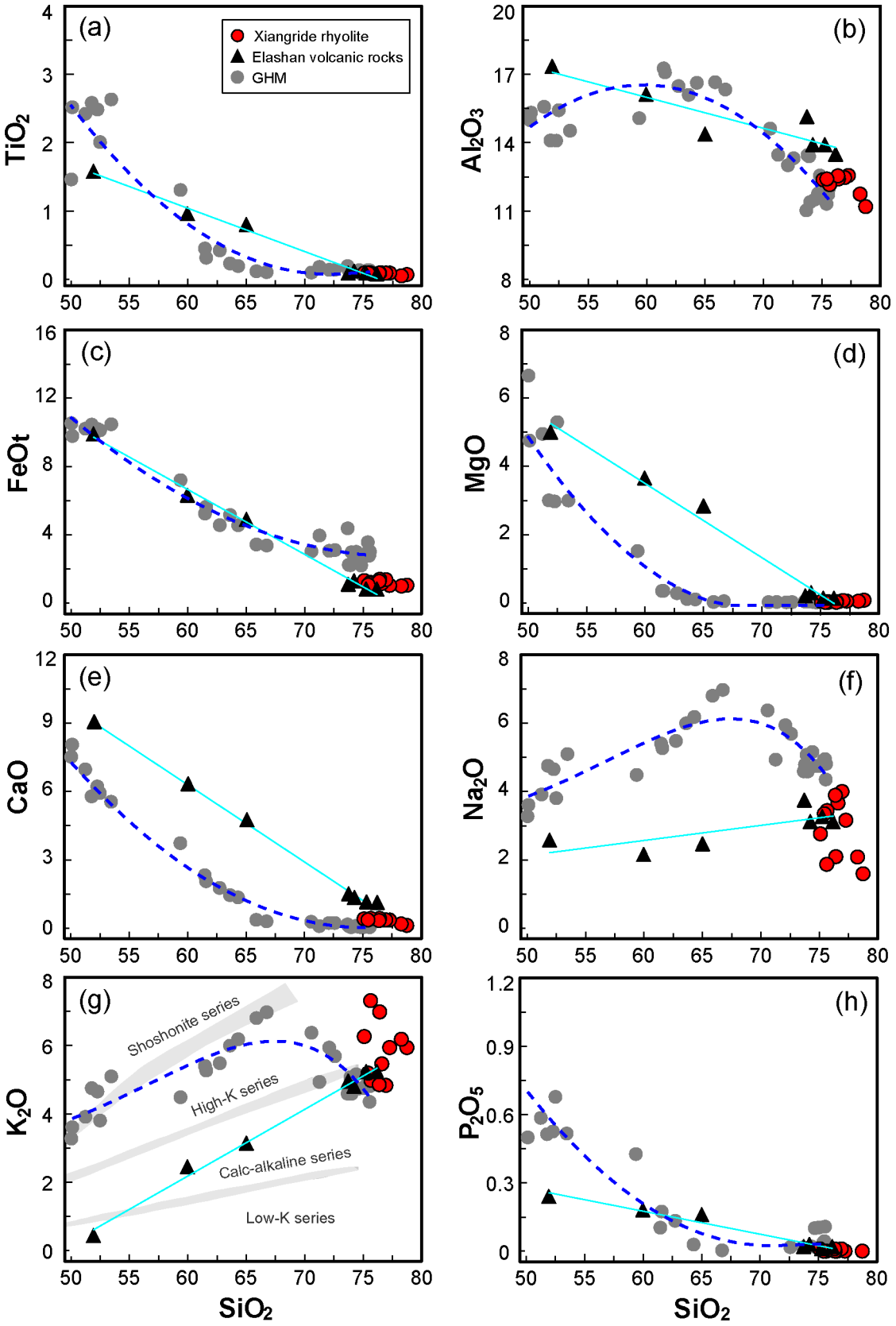

Fig. 5. SiO_2 variation diagrams for major element oxides. The solid line is the liquid line of descent defined by the Elashan volcanic association, which differs from that of the GHM volcanic rocks (the dashed curve).

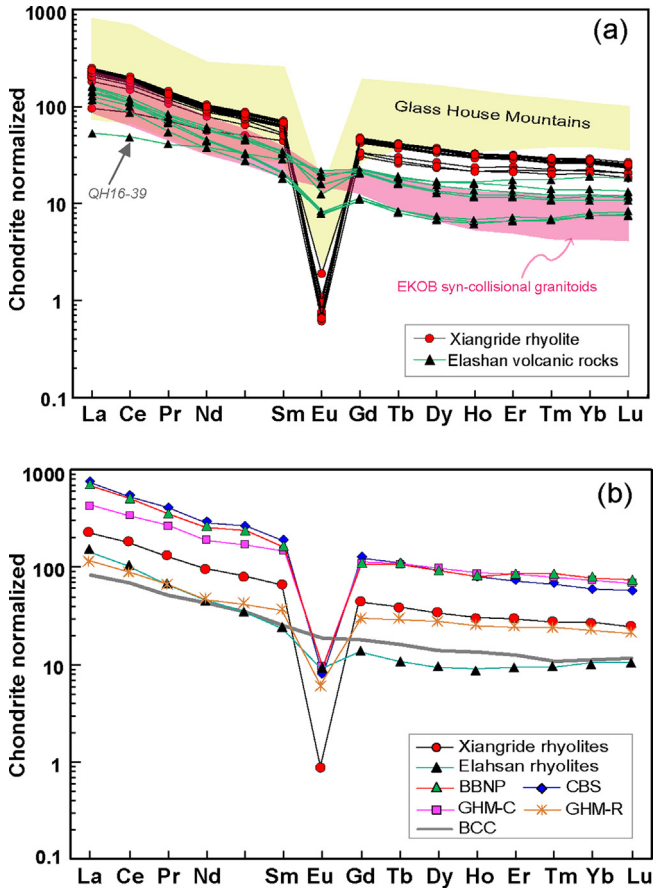

Fig. 6. (a) Chondrite-normalized (after Sun and McDonough, 1989) REE patterns for the Triassic volcanic rocks in the EKOB. For composition, the compositions of the GHM rhyolites are also showed. The REE contents of Elashan volcanic rocks are much lower than Xiangride rhyolites that is similar to the GHM rhyolites. (b) REE patterns of average peralkaline rhyolites (CBS, BBNP, GHM-C), peraluminous rhyolites (GHM-R) and model bulk continental crust are plotted together with Triassic volcanic rocks in the EKOB for comparison. The globally typical peralkaline rhyolites are BBNP (Big Bend National Park comendites, n = 4; after Parker et al., 2012), CBS (Chang Bai Shan comendites, n = 5; after Chen, 2013), and GHM-C (GHM comendites, n = 16; after Shao et al., 2015). Also, GHM-R (GHM peraluminous rhyolites, n = 2; after Shao et al., 2015) and BCC (bulk continental crust; Rudnick and Gao, 2003) are plotted for comparison.

However, it should be noted that the P.I. (Fig. 4b) and REE patterns (Fig. 6a) of the felsic Elashan volcanic rocks are similar to those of spatially adjacent Triassic *syn*-collisional granitoids in the EKOB (Fig. 1c). These widespread granitoids intruded earlier (250–220 Ma; Huang et al., 2014; Xia et al., 2014; Shao et al., 2017) than the Elashan volcanic rocks erupted (232–217 Ma; Hu et al., 2016; Xu et al., 2019, 2020a). The close temporal and spatial associations of these felsic igneous rocks offer convincing evidence that these rocks are genetically related. Fig. 9 shows that the initial $^{87}Sr/^{86}Sr$ ratios and $\varepsilon_{Nd}(t)$ values of the Elashan volcanic rocks are identical to those of the *syn*-collisional granitoids and that their the $\varepsilon_{Hf}(t)$ values also overlap. The Sr-Nd-Hf isotopes also imply that the source of these volcanic rocks may be the same as that of the *syn*-collisional granitoids. Thus, we conclude that the felsic Elashan volcanic rocks and the *syn*-collisional granitoids are different products of the same magmatic event, which occurred in response to continental collision. The felsic Elashan volcanic rocks are the same as the widespread granitoids, but they are erupted melts with more evolved compositions. Huang et al. (2014) and Shao et al. (2017) demonstrated that the Triassic *syn*-collisional granitoids in the EKOB originated by partial melting of the last fragments of the underthrust Anyemaqen oceanic upper crust under amphibolite facies conditions (see details in Mo et al., 2008; Niu et al., 2013). We infer that the underthrust Paleo-Tethys oceanic crust is also the most probable candidate for the source of the felsic Elashan volcanic rocks. Based on the research conducted on the Linzizong volcanic succession (~65–45 Ma) in southern Tibet, Mo et al. (2008) and Niu et al. (2013) proposed that the oceanic crust and sediment/mature crustal material melted during and soon after the collision under the amphibolite facies conditions.

We conducted simple Nd-Hf mass balance calculations to estimate the relative contributions of the oceanic crust and mature crustal material to the source of the felsic Elashan volcanic rocks. We choose two end members: (i) the Paleo-Tethys MORB from the Jinshajiang suture (Xu and Castillo, 2004) represents the oceanic upper crust, (ii) and the Paleoproterozoic granitic gneiss from the EKOB (Shao et al., 2017) represents the mature continental crustal materials. Fig. 9c shows that melting of source rocks equivalent to ~75%–80% Paleo-Tethys MORB and ~20%–25% mature continental crustal material can explain the petrogenesis of the felsic Elashan volcanic rocks. Upon collision, the cold Anyemaqen oceanic crust was underthrust and slowly attained thermal equilibrium with the prior hot active continental margin, thus evolving along a high T/P geothermal path. The warm and highly hydrated oceanic crust (along with minor terrestrial sediments) melted when they reached the hydrous basaltic solidus under amphibolite conditions, producing andesitic parental melts of the Triassic *syn*-collisional granitoids and the felsic Elashan volcanic rocks.

Fig. 8 shows that the Nb*-Ta* anomalies and the Nb/Ta ratio (17.22) of basalt QH16-39 are close to those of mantle-derived magmas. The isotopic data for basalt QH16-39 (lower initial $^{87}Sr/^{86}Sr$, higher $^{206}Pb/^{204}Pb$ and $^{208}Pb/^{204}Pb$, and $\varepsilon_{Hf}(t) > 1$) are also consistent with a mantle origin. We speculate that basalt QH16-39 may have been formed by decompression melting of the asthenospheric mantle due to post-collisional extension, and we are currently looking for further geochronologic evidence.

5.2. Petrogenesis of the Xiangride rhyolites

5.2.1. Was the high Nb-Ta characteristic inherited from the mantle source?

The Xiangride rhyolites have significantly higher Nb-Ta contents and Nb/Ta ratios than the felsic Elashan volcanic rocks, resembling GHM peralkaline rhyolites (Figs. 7, 8b). The mantle-derived peralkaline rhyolites from the GHM area and elsewhere (Kar et al., 1998; Peccerillo et al., 2003, 2007; Mbassa et al., 2012; White et al., 2012; Hutchison et al., 2016; Chandler and Spandler, 2020) characteristically have high Nb-Ta contents. Bailey and Macdonald (1975, 1987) suggested that the halogens, Na, Zr, Nb, Ta, and other elements abundant in peralkaline felsic melts can be enriched by magmatic vapors ascending from the mantle or deep crust. The element transfer mechanism from vaper to melt is confusing, and analysis of melt inclusions in pantellerites have revealed that they do not have detectable elements such as Zr, Nb, Ta, and Y contents (Lowenstern and Mahood, 1991). Agangi et al. (2010) demensteated that accessary minerals account for the high concentrations of some lithophile elements (REEs, Y, and HFSEs) in rhyolites due to the postponed accessory mineral crystallization caused by mantle-derived F-rich fluids. F-rich fluids could transport HFSEs to some extent in the form of complexes (e.g., K_2TiF_6) or could change the melt structure in magmatic hydrothermal fluid systems and subduction zones (e.g., Bailey, 1977; Keppler, 1993; Martin, 2006; He et al., 2015; Macdonald et al., 2019). We infer that the high Nb and Ta contents of the Xiangride rhyolites were probably inherited from primary magmas from a Nb-Ta enriched source or were achieved through magmatic evolution. Ding et al. (2011) evaluated whether the fractional crys-

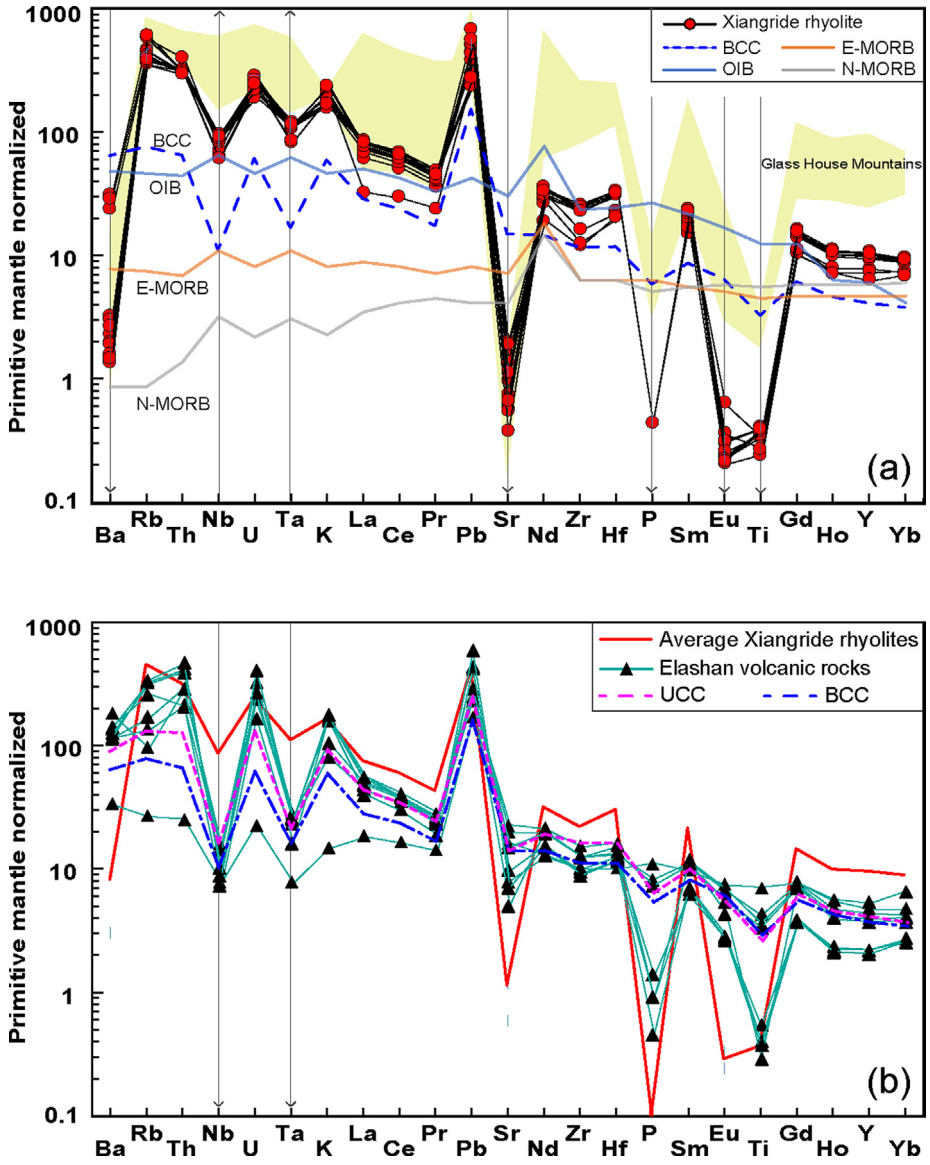

Fig. 7. (a) Primitive mantle (after Sun and McDonough, 1989) normalized multi-element diagrams to show that the Xiangride rhyolites have high content of most incompatible elements (especially high Nb and Ta inherited from their parental alkali basalt), but strong Ba, Sr, Eu, P, and Ti depletion, resembling those of peralkaline rhyolites from the GHM area. Average OIB, E-MORB, N-MORB, and bulk continental crust (BCC) are plotted for composition (after Sun and McDonough, 1989; Rudnick and Gao, 2003). (b) The Elashan volcanic rocks exhibit obvious Nb and Ta negative anomalies, resembling the model bulk continental crust and upper continental crust (UCC) compositions (after Rudnick and Gao, 2003). The Xiangride rhyolites (mean, n = 13) have stronger Ba, Sr, Eu, P and Ti depletion than Elashan rhyolites and continental crust.

tallization of mineral assemblages (amphibole, plagioclase, alkali feldspar, quartz, ilmenite, titanomagnetite, and apatite) could significantly reduce or increase the Nb and Ta contents of magmas. Simple fractional crystallization calculations for an andesitic magma (SiO_2 = 60 wt.%) revealed that the effect of the fractional crystallization of certain mineral assemblages is weak. That is, it is difficult to achieve the high Nb and Ta contents of the Xiangtide rhyolites through magmatic differentiation. Thus, the high Nb-Ta contents of the Xianagride rhyolites were most likely inherited from a Nb-Ta enriched source.

Niu and Batiza (1997) demonstrated that $D_{Nb} \approx D_{Th} < D_{Ta} \approx D_U$ during mantle melting and much of basaltic magma evolution (e.g., olivine-clinopyroxene-plagioclase crystallization), indicating that the Nb/Th and Ta/U ratios do not change during magmatic processes. It follows that the varying Nb/Th and Ta/U ratios (or Nb* and Ta*) of magmatic rocks must be inherited from their sources or source histories. Because Nb and Ta are enriched (Nb *vs.* Th; Ta *vs.* U) in strictly mantle-derived basaltic magmas (e.g., OIB, E-MORB, and N-MORB) and are depleted in subduction and collision zone magmas (Niu and O'Hara, 2003), the mantle-derived magmas are concentrated in the upper right quadrant, with both Nb* >1 and Ta* >1, while the collisional granitoids and arc rhyolites plot in the lower left quadrant, with Nb* and Ta* < 1 (Fig. 8a) (Ewart et al., 1998; Sui et al., 2013; Chen et al., 2014; Shao et al., 2017). The Nb-Ta depletions of subduction zone magmas are widely believed to result from rutile (rich in Ti, Nb, and Ta) retention in the subducting slab as it undergoes dehydration and induces mantle wedge melting. Since of the water-bearing minerals, Nb and Ta have higher affinity to amphibole, the Nb-Ta depletions in collisional granites is probably produced by residual amphibole (and minor ilmenite) because of high Kd_{Nb} and Kd_{Ta} of amphibole (Foley et al., 2002) and high amphibole modal proportion of the magmatic sources (~66.4%; i.e., mineral mode of amphibolite of MORB protolith; Niu and O'Hara, 2009). As Nb and Ta are strongly

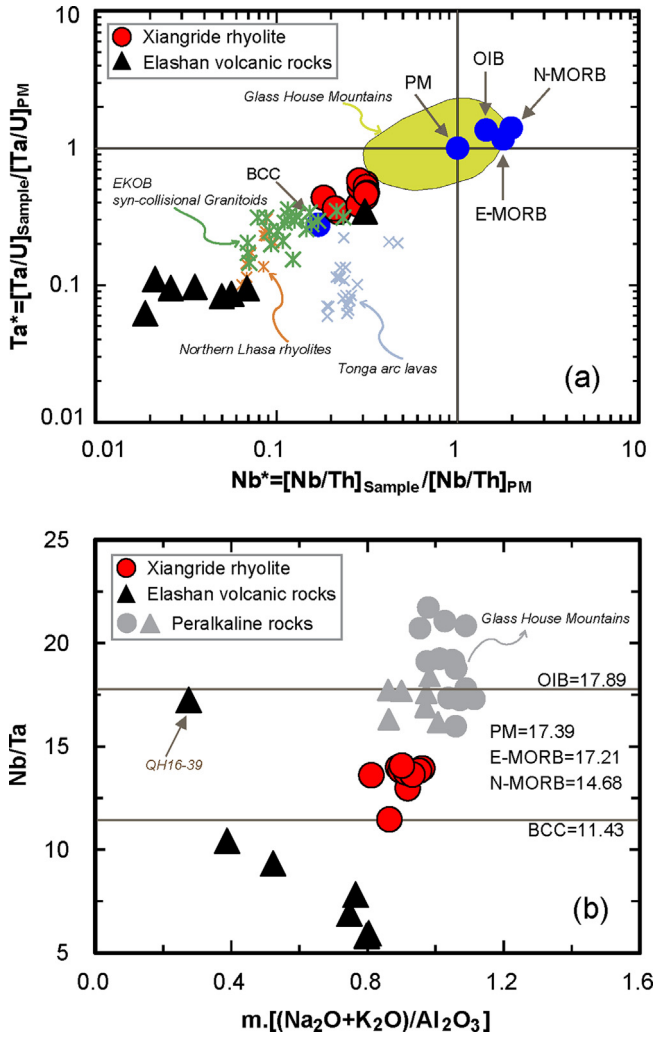

Fig. 8. (a) Nb*–Ta* anomaly diagram (after Niu et al., 1999). The distinctively high Nb (*vs.* Th) and Ta (*vs.* U) of the Xiangride rhyolites are inherited from their parental melts with high Nb and Ta. Crustal rocks, which have too low Nb and Ta, plot in the lower left quadrant. (b) The Nb/Ta ratios of the Xiangride rhyolites and the basalt QH16-39 from the Elashan area are comparable with mantle derived melts, while the Nb/Ta ratios of the felsic Elashan volcanic rocks are even lower than that of the upper continental crust. Data for average OIB, N-MORB, E-MORB (after Niu and O'Hara, 2003), primitive mantle (PM, after Sun and McDonough, 1989), upper continental crust (UCC, after Rudnick and Gao, 2003), Glass House Mountains (after Shao et al., 2015), peraluminous rhyolites from the Northern Lhasa terrane (after Sui et al., 2013; Chen et al., 2014), Tonga are lava (after Ewart et al., 1998), and peraluminous granites from the EKOB (after Shao et al., 2017) are plotted for comparation.

depleted in crustal rocks, partial melting of crustal rocks or fractional crystallization of crust-derived magmas are unlikely to produce melts with the Nb*-Ta* values similar to those of the Xiangride rhyolites. Due to the high Nb* and Ta* inherited from the parental alkali basaltic melts, typical peralkaline rhyolites (GHM) plot close to Nb* = 1 and Ta* = 1 (Fig. 8a). The Xiangride rhyolites plot between typical peralkaline rhyolites and the BCC, with Nb* and Ta* < 1. Thus, we infer that the parental melts of the Xiangride rhyolites were largely basaltic melts of mantle peridotite, but continental crust contamination (see below) resulted in Nb* and Ta* < 1 because of the negative Nb and Ta anomalies of crustal rocks.

5.2.2. Evidence from Sr-Nd-Pb-Hf isotopes

The pre-existing old crustal rocks in the study area are the granitic gneiss of the Paleoproterozoic basement (i.e., the Baishahe Formation), which have higher Sr isotope ratios and lower Nd and Hf isotopes (granitic gneiss, ~2.1 Ga, initial $^{87}Sr/^{86}Sr$ = 0.749253, $\varepsilon_{Nd}(t)$ = −17.22, $\varepsilon_{Hf}(t)$ = −15.91; Shao et al., 2017) than the Xiangride rhyolites. Thus, these ancient crustal rocks cannot be the main source of the Xiangride rhyolites. Because of its strong U and Th depletions, the lower crust has very low Pb isotope ratios ($^{206}Pb/^{204}Pb \approx 14.0$, $^{207}Pb/^{204}Pb \approx 14.7$; Rollinson, 1993; Rudnick and Gao, 2003), we can exclude the possibility that the Xiangride rhyolites originated from the lower crust based on their Pb isotope ratios ($^{206}Pb/^{204}Pb$ = 18.25–18.43; $^{208}Pb/^{204}Pb$ = 35.96–37.78). The Rb-Sr isochron age of the Xiangride rhyolites (207.4 Ma; Fig. 9b) is essentially the same as the U-Pb zircon ages reported in this paper (208.4 ± 1.6 Ma and 209.1 ± 0.7 Ma; Fig. 3) and by reference Ding et al. (2011) (213 Ma). The calculated initial $^{87}Sr/^{86}Sr$ (0.70510; Fig. 9b) indicates that the primitive magma parental to these rhyolites may have been derived from mantle sources with low $^{87}Sr/^{86}Sr$ (Sun and McDonough, 1989). Remarkably, the Nd and Hf isotopic data also suggest that there must have contribution from continental crust contamination (Fig. 9c).

All of the above isotopic features, together with the Nb-Ta enrichment, indicate that the origin of the Xiangride rhyolites is similar to that of typical peralkaline rhyolites, i.e., protracted fractional crystallization of alkali-rich basaltic melts plus the effects of continental crust contamination (Shao et al., 2015; Hutchison et al., 2016; Chandler and Spandler, 2020). The most likely contamination mechanisms are a combination of crustal assimilation and magmatic fractional crystallization (AFC) between basaltic magma and the crust (Depaolo, 1981; Reiners et al., 1995; Nishimura, 2012; Deniz and Kadioglu, 2016; Burton-Johnson, et al, 2019). Without considering the initial temperature difference and energy variation in the magma-country-rock system, we conducted simple quantitative calculations using the AFC model established by Depaolo (1981) to estimate the relative contributions of the crust and mantle to the petrogenesis of the Xiangride rhyolites in terms of several representative trace elements (Fig. 10). (i) As the Xiangride rhyolites have significantly characteristics resembling the typical peralkaline rhyolites that originated form protracted fractional crystallization of OIB-like alkali-rich basaltic melts, we choose OIB as the initial magma source in AFC modeling. The modeled parental magma composition was typical oceanic island basalt (OIB; Sun and McDonough, 1989) and the assimilate composition was that of lower continental crust (LCC; Rudnick and Gao, 2003). (ii) The ratio of the rates of assimilation and crystallization (r) was assumed to be 0.5 (Reiners et al., 1995). (iii) The simplified mineral modes were 15% olivine, 10% clinopyroxene, 15% hornblende, 35% plagioclase, 15% alkali plagioclase, 5% quartz, 2% titanomagnetite, 2% ilmenite, and 1% apatite; and the mineral partition coefficients used were those of the Geochemical Earth Reference Model (http://earthref.org/KDD/). The calculations revealed that a basaltic magma that undergoes 20%–30% crystallization (i.e., F = 0.8–0.7) with 10%–15% crustal assimilation can produce a magma with Nb, Ce, Nd, Hf, Gd, Ho, and Lu contents close to those of the Xiangride rhyolites (Fig. 10). Therefore, we infer that the best candidate for the source magma of the Xiangride rhyolites is asthenospheric mantle derived alkali basaltic magma that underwent protracted fractional crystallization in a crustal magma chamber, which gave rise to the crustal assimilation signature.

5.3. Tectonic implications for the Qinling, Qilian and Kunlun orogenic belts

The Anyemaqen Ocean probably closed in the Late Permian to Early Triassic (Yang et al., 2009), and then, the continental collision of the Qaidam terrane and Songpan-Garze terrane occurred, resulting in the generation of the widespread *syn*-collisional granitoids and felsic volcanic rocks (Fig. 11a–b). As was discussed above,

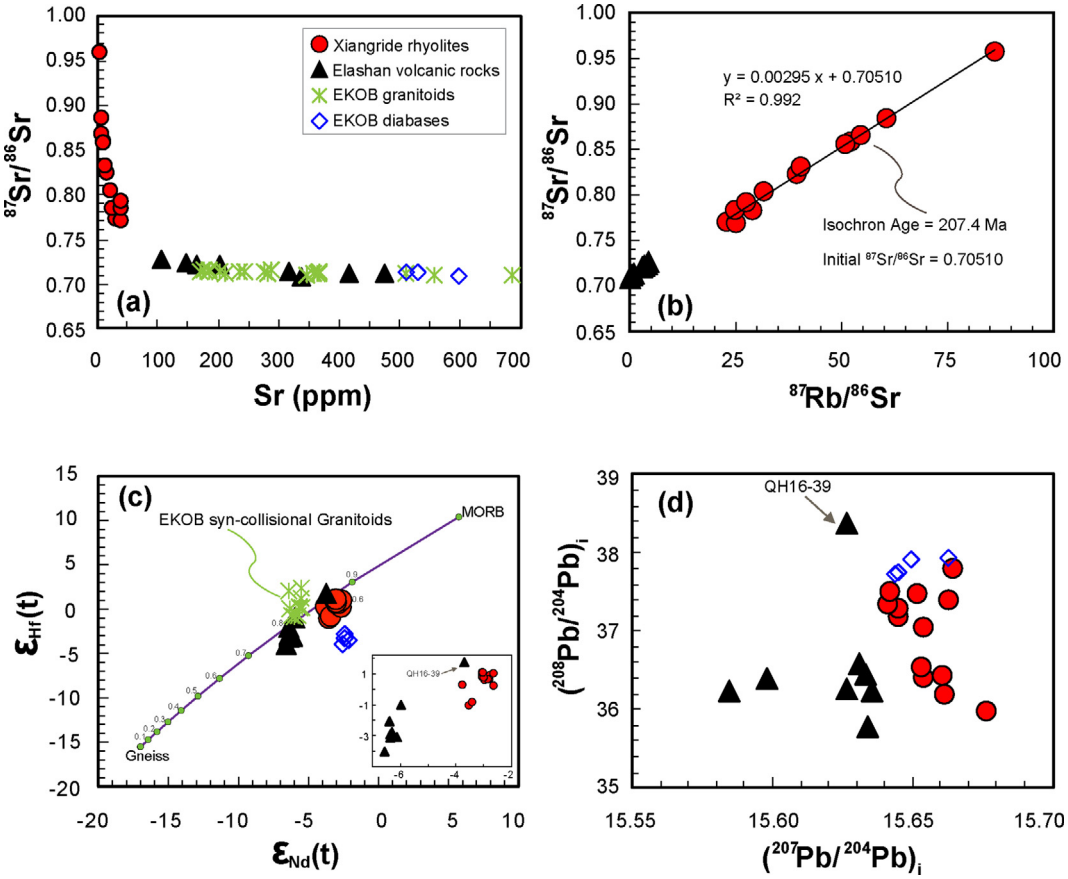

Fig. 9. (a) $^{87}Sr/^{86}Sr$ ratios of the Xiangride rhyolites increase with decreasing Sr. Highly fractionated rhyolites with high Rb/Sr have extremely high $^{87}Sr/^{86}Sr$ ratios because almost all of the Sr are radiogenic ^{87}Sr resulting from ^{87}Rb decay. $^{87}Sr/^{86}Sr$ of the Elashan volcanic rocks are compatible with Triassic granitoids of the EKOB (after Shao et al., 2017). Data of Late Triassic diabasic dikes from the EKOB (after Hu et al., 2016) were also plotted for comparation. (b) The Xiangride rhyolites define a Rb-Sr isochron age of 207.4 Ma, which is consistent with the U-Pb zircon age (208.4 Ma and 209.1 Ma), with the initial $^{87}Sr/^{86}Sr$ of 0.7051 lower than that of the Elashan volcanic rocks (0.71062). (c) The $\varepsilon_{Nd}(t)$ *vs.* $\varepsilon_{Hf}(t)$ diagram. $\varepsilon_{Nd}(t)$ and $\varepsilon_{Hf}(t)$ of the Xiangride rhyolites are similar to those of the diabasic dikes. Simple mass balance calculation shows that the source rocks of the felsic Elashan volcanic rocks are equivalent to mixing of ~75–80% Paleo-Tethys MORB (Nd = 6.2 ppm, Hf = 1.31 ppm, $\varepsilon_{Nd}(t)$ = 5.74, $\varepsilon_{Hf}(t)$ = 10.41; after Xu and Castillo, 2004) and ~20%–25% mature crustal material (Proterozoic granitic gneiss; Nd = 28.0 ppm, Hf = 4.7 ppm, $\varepsilon_{Nd}(t)$ = −17.22, $\varepsilon_{Hf}(t)$ = −15.91; after Shao et al., 2015). (d) Initial $^{207}Pb/^{204}Pb$ ratios of the Xiangride rhyolites resembling the diabasic dikes are higher than that of felsic volcanic rocks from the Elashan Formation, while the basalt QH 16–39 has the highest initial $^{208}Pb/^{204}Pb$ ratio.

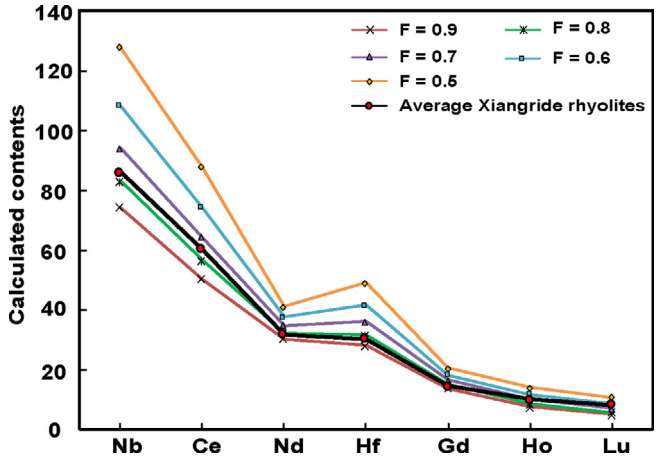

Fig. 10. The modeled AFC (after Depaolo,1981) path for Xiangride rhyolites in terms of several representative trace elements. Modeled parent magma and assimilate compositions were OIB (after Sun and McDonough, 1989) and lower continental crust (after Rudnick and Gao, 2003) respectively. The ratio of rates of assimilation and crystallization (r) was assumed to be 0.5 (after Reiners et al., 1995). The simplified mineral modes were 15% olivine, 10% clinopyroxene, 15% hornblende, 35%plagioclase, 15% alkali plagioclase, 5% quartz, 2% titanomagnetite, 2% ilmenite, and 1% apatite, and the mineral partition coefficients used were those of the Geochemical Earth Reference Model (http://earthref.org/KDD/).

the Triassic calc-alkaline felsic volcanic rocks and the *syn*-collisional granitoids are different products of the same magmatic event, which occurred in response to this collision. The stratigraphic records indicate that the continental collision was basically completed in the early stage of Late Triassic, resulting in folding and thrusting in the EKOB (Fig. 11c–d) (Guo et al., 1998; Luo et al., 2002; Li et al., 2012; Xu et al., 2013). However, the exact transition time from collisional compression to post-collisional extension is controversial. Based on geochemical characteristics and the U-Pb zircon ages of local Triassic igneous rocks in the EKOB, Xiong et al. (2014), Ren et al. (2016), and Zhao et al. (2020) proposed that the tectonic transformation occurred at 223 Ma, 226 Ma, and <225 Ma, respectively. Chen et al. (2019b) suggested that the peak formation time (230 Ma) of the Late Paleozoic–Early Mesozoic metallogenic deposits in the EKOB corresponds to the tectonic transition from *syn*-collision to post collision. Based on evidences from ophiolitic mélanges and related volcanic rocks, intrusive plutons, and sedimentary cover sequences, Dong et al. (2018) proposed that the EKOB underwent post-collisional collapse and extension and generated the A-type granites and andesitic-rhyolitic volcanics in the upper Triassic Elashan Formation at ~220–200 Ma. There are abundant alkaline diabasic dikes (218.1 ± 2.5 Ma; Fig. 4) intruding the A-type granitoids in the western section of the EKOB (Hu et al., 2016). These highly evolved alkaline basaltic rocks are very similar to the inferred

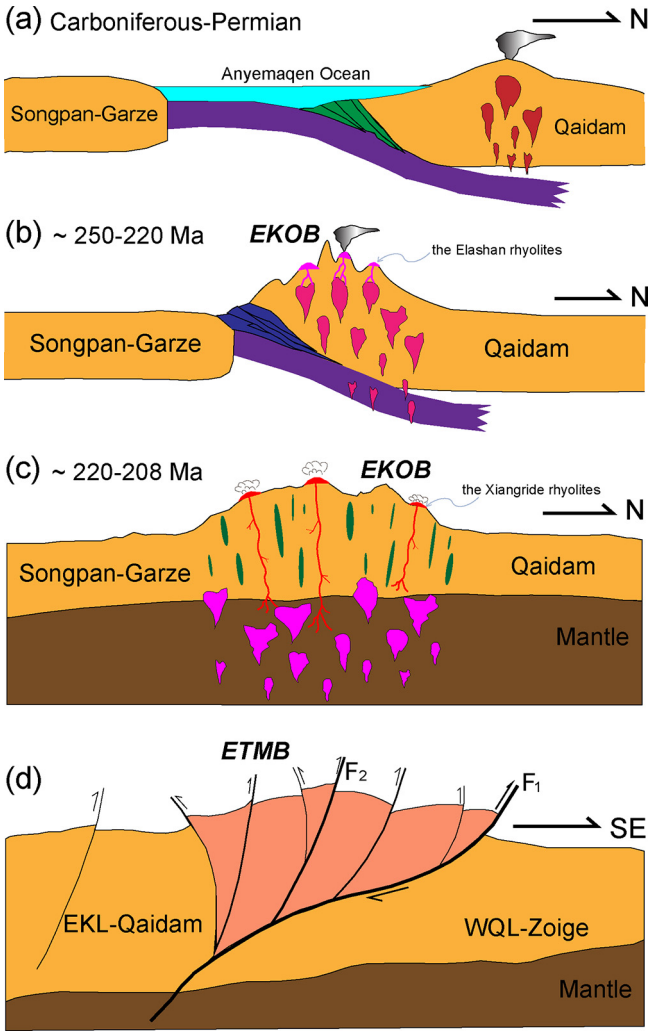

Fig. 11. Cartoons showing the formation of the EKOB and the Elashan tectonic-magma belt (ETMB) from the Late Paleozoic to Early Mesozoic. (a) Subduction of Anyemaqen seafloor and related arc magmatism in the Carboniferous to Permian. (b) Collision of the Songpan-Garze terrane with the Qaidam terrane in the Early–Middle Triassic and the consequent magmatism for *syn*-collisional granitoids and felsic volcanic rocks of the Elashan Formation. (c) The occurrence of mafic dikes and peralkaline-like Xiangride rhyolites in the Late Triassic due to post-collisional lithosphere extension. (d) Formation of the ETMB in the Late Triassic according to the A-type subduction of the West Qinling-Zoige massive (after Zhang et al., 2000). F_1 is the major detachment surface and F_2 (Wenquan fault/Elashan fault; Fig. 1b) is one of the secondary thrusting faults.

mafic parental melts of the peralkaline-like Xiangride rhyolites. Fig. 9 shows that the Sr-Nd-Hf-Pb isotopic data of these diabasic dikes are similar to the Xiangride rhyolites. Thus, we conclude that the Xiangride rhyolites and the mafic dikes may be different products of the same thermal event and their primitive parental magmas were derived from the asthenosphere mantle due to post-collisional extension. Here, we provide petrological evidence for tectonic transformation from a *syn*-collisional environment to a post-collisional environment in the EKOB. That is, the rock types from the early granitoids and calc-alkaline volcanic rocks (~250–220 Ma) to the late alkaline basaltic dikes and peralkaline-like rhyolites (~218–209 Ma) provide important information about the tectonic evolution of the EKOB and we infer that the transition point from collisional compression to post-collisional extension occurred at ~220 Ma. The Elashan tectonic-magmatic belt (ETMB; Zhang et al., 2000), which is bounded by several left-lateral oblique-thrust faults between West Qinling and East Kunlun (Fig. 11d), lies at the triple junction of the Qinling-Qilian-Kunlun orogenic belts (Fig. 1b), and the Elashan/Wenquan fault is often regarded as the boundary between East Kunlun and West Qinling. Considering that (i) the main geological records of the Qilian Orogen represent the Early Paleozoic Caledonian system (Song et al., 2013); (ii) the *syn*-collisional granitoids of the Qinling Orogen (~220 Ma) are slightly younger than those of the ETMB (Li et al., 2015c; Duan et al., 2016; Kong et al., 2017, 2019a); (iii) the Permian-Triassic granitoids and volcanic rocks that outcropped in the ETMB are comparable with those in the EKOB (Xia et al., 2014; Ren et al., 2016; Kong et al., 2020; Zhao et al., 2020); and (4) the ETMB has the same Proterozoic crystalline basement as the EKOB (Sun, 2004; Chen, 2015), we infer that the ETMB has the best affinity with the EKOB and should be considered to be part of the EKOB. Fig. 11 illustrates the evolution of the ETMB. The main body of the EKOB was formed by the northward subduction of the Anyemaqen Ocean (Fig. 11a) (Yin and Zhang, 1998) and the subsequent collision between the Qaidam terrane and the Songpan-Garze terrane (Fig. 11b), causing the EKOB to combine with the Qaidam terrane. The easternmost part of the EKOB (i.e., the ETMB) was also reformed by the NW-SE oblique obduction of the eastern part of the EKOB-Qaidam massif, and the main terrestrial stress came from the SE–NW A-type subduction of the West Qinling-Zoige massif (Fig. 11d) (Zhang et al., 2000). Horizontally, the ETMB exhibits left-lateral strike-slip motion due to the passive drag of the oblique-thrusting. A series of left-lateral strike-slip faults increased the N–S extension of the ETMB by ~100 km (Fig. 1b). At the same time, these faults affect the distribution direction of the collisional intrusions and extrusions, making them parallel to the Elashan fault (Fig. 1c).

6. Conclusions

(i) The petrogenesis of the widespread Triassic calc-alkaline felsic volcanic rocks (~232–225 Ma) is consistent with an origin of partial melting of the underthrust Paleo-Tethys oceanic crust under amphibolite facies conditions.

(ii) The peralkaline-like Xiangride rhyolites (~209 Ma) originated from an asthenospheric mantle derived alkali basaltic magma that underwent protracted fractional crystallization and continental crust contamination.

(iii) According to the rock types from the granitoids and calc-alkaline volcanic rocks to alkaline basaltic dikes and peralkaline-like rhyolites, we infer that the transition from collisional compression to post-collisional extension occurred at about 220 Ma.

Declaration of Competing Interest

The authors declare that they have no known competing financial interests or personal relationships that could have appeared to influence the work reported in this paper.

Acknowledgements

We thank Di Hong and Yajie Gao for field operation and Mengni Zeng for sample preparation. We thank Xiaohong Wang, Hongmei Gong, Yuanyuan Xiao, Pu Sun and Meng Duan for laboratory assistance in geochemistry and isotope analysis. We appreciate anonymous reviewers for constructive comments, Editorial Advisor Prof. M. Santosh and Associate Editor Prof. Wenjiao Xiao for handing this manuscript. This work was mainly supported by National Natural Science Foundation of China (NNSF, Grant No. 41803028) and Natural Science Foundation of Shandong Province (NSFSP, Grant No. ZR2018BD020) to Fengli Shao. Other grants (Grant Nos. 41802201, 41630968 and 41688103 from NNSF, Grant

Nos. ZR2018BD012 and ZR2020QD044 from NSFSP, and Grant No. 2019RZA02002 from soft science project of Shandong Province Key Research and Development Plan) also provide assistance.

Appendix A. Supplementary data

Supplementary data to this article can be found online at https://doi.org/10.1016/j.gsf.2021.101243.

References

Agangi, A., Kamenetsky, V.S., McPhie, J., 2010. The role of fluorine in the concentration and transport of lithophile trace elements in felsic magmas: insights from the Gawler range volcanics, South Australia. Chem. Geol. 273, 314–325.

Adam, J., Green, H.T., Sie, S.H., 1993. Proton microprobe determined partitioning of Rb, Sr, Ba, Y, Zr, Nb and Ta between experimentally produced amphiboles and silicate melts with variable F content. Chem. Geol. 109, 29–49.

Bailey, D.K., Macdonald, R., 1975. Fluorine and chlorine in peralkaline liquids and the need for magma generation in an open system. Mineral. Mag. 40, 405–414.

Bailey, D.K., Macdonald, R., 1987. Dry peralkaline felsic liquids and carbon dioxide flux through the Kenya Rift dome. In: Mysen, B. (Ed.), Magmatic processes: physicochemical principles. The Geochemical Society (Spec. Pub.), pp. 91–105..

Bailey, J.C., 1977. Fluorine in granitic rocks and melts: a review. Chem. Geol. 19, 1–42.

Black, S., Macdonald, R., Kelly, M.R., 1997. Crustal origin for peralkaline rhyolites from Kenya: evidence from U-series disequilibria and Th-isotope. J. Petrol. 38, 227–297.

Bohrson, W.A., Reid, M.R., 1997. Genesis of silicic peralkaline volcanic rocks in an ocean island setting by crustal melting and open-system processes: Socorro Island. Mexico. J. Petrol. 38, 1137–1166.

Burton-Johnson, A., Macpherson, C.G., Ottley, C.J., Nowell, G.M., Boyce, A.J., 2019. Generation of the Mt Kinabalu granite by crustal contamination of intraplate magma modelled by equilibrated major element assimilation with fractional crystallization (EME-AFC). J. Petrol. 60, 1461–1487.

Chandler, R., Spandler, C., 2020. The igneous petrogenesis and rare metal potential of the peralkaline volcanic complex of the southern Peak Range, Central Queensland, Australia. Lithos 358–359. https://doi.org/10.1016/j.lithos.2020.105386 105386.

Chen, G.C., Pei, X.Z., Li, R., Li, Z.C., Pei, L., Liu, C.J., Chen, Y.X., Wang, M., 2019b. Late Paleozoic-Early Mesozoic tectonic-magmatic evolution and mineralization in the eastern section of the East Kunlun Orogenic Belt. Acta Geol. Sinica (English Edition) 93 (suppl. 2), 158–159.

Chen, G.C., Pei, X.Z., Li, R., Li, Z.C., Pei, L., Liu, C.J., Chen, Y.X., Wang, M., Gao, F., Li, X.B., 2019a. Lithospheric extension of the post-collision stage of the Paleo-Tethys oceanic system in the East Kunlun Orogenic belt: insights from Late Triassic plutons. Earth Sci. Front. 26, 191–208 (in Chinese with English abstract).

Chen, N.S., Wang, Q.Y., Chen, Q., Li, X.Y., 2007. Components and metamorphism of the basements of the Qaidam and Oulongbuluke micro-continental blocks and a tentative interpretation of paleocontinental evolution in NW-Central China. Earth Sci. Front. 14, 43–55 (in Chinese with English abstract).

Chen, S., Wang, X.H., Niu, Y.L., Sun, P., Duan, M., Xiao, Y.Y., Guo, P.Y., Gong, H.M., Wang, G.D., Xue, Q.Q., 2017. Simple and cost-effective methods for precise analysis of trace element abundances in geological materials with ICP-MS. Sci. Bull. 62, 277–289.

Chen, X., 2013. Petrography and Geochemistry Indication of Crystallization Differentiation and Magma Mixing Process of the Tianchi Volcano, Changbaishan M.S. thesis. China Earthquake Administration, Beijing, pp. 1–121 (in Chinese with English abstract).

Chen, Y., 2015. The composition and geological evolution of Pre-Cambrian Metamorphic rocks in east region of East Kunlun orogenic belt Ph.D. thesis. Chang'an University, pp. 1–147 (in Chinese with English abstract).

Chen, Y., Zhu, D.C., Zhao, Z.D., Meng, F.Y., Wang, Q., Santosh, M., Wang, L.Q., Dong, G. C., Mo, X.X., 2014. Slab breakoff triggered ca. 113 Ma magmatism around Xainza area of the Lhasa Terrane, Tibet. Gondwana Res. 26, 449–463.

Deniz, K., Kadioglu, Y.K., 2016. Assimilation and fractional crystallization of foid-bearing alkaline rocks: Buzlukdağ intrusives, Central Anatolia, Turkey. Turkish J. Earth. Sci. 25, 341–1332.

DePaolo, D.J., 1981. Trace element and isotopic effects of combined wall-rock assimilation and fractional crystallization. Earth Planet. Sci. Lett. 52, 177–184.

Ding, S., Huang, H., Niu, Y.L., Zhao, Z.D., Yu, X.H., Mo, X.X., 2011. Geochemistry, geochronology and petrogenesis of East Kunlun high Nb-Ta rhyolites. Acta Petrol. Sin. 27, 3603–3614 (in Chinese with English abstract).

Dong, Y.P., He, D.F., Sun, S.S., Liu, X.M., Zhou, X.H., Zhang, F.F., Yang, Z., Cheng, B., Zhao, G.C., Li, J.H., 2018. Subduction and accretionary tectonics of the East Kunlun orogen, western segment of the Central China Orogenic System. Earth Sci. Rev. 186, 231–261.

Duan, M., Niu, Y.L., Kong, J.J., Sun, P., Hu, Y., Zhang, Y., Chen, S., Li, J.Y., 2016. Zircon U-Pb geochronology, Sr-Nd-Hf isotopic composition and geological significance of the Late-Triassic Baijiazhuang and Lvjing granitic plutons in western Qinling Orogen. Lithos 260, 443–456.

Ewart, A., Collerson, K.D., Regelous, M., Wendt, J.I., Niu, Y., 1998. Geochemical evolution within the Tonga–Kermadec–Lau Arc–Back-arc Systems: the role of varying mantle wedge composition in space and time. J. Petrol. 39, 331–368.

Ewart, A., Griffin, W.L., 1994. Application of proton-microprobe data to trace-element partitioning in volcanic rocks. Chem. Geol. 117, 251–284.

Foley, S., Tiepolo, M., Vannucci, R., 2002. Growth of early continental crust controlled by melting of amphibolite in subduction zones. Nature 417, 837–840.

Gong, S.L., Chen, N.S., Wang, Q.Y., Kusky, T.M., Wang, L., Zhang, L., Ba, J., Liao, F.X., 2012. Early Paleoproterozoic magmatism in the Quanji Massif, northeastern margin of the Qinghai-Tibet Plateau and its tectonic significance: LA-ICPMS U-Pb zircon geochronology and geochemistry. Gondwana Res. 21, 152–166.

Guo, Z.F., Deng, J.F., Xu, Z.Q., Mo, X.X., Luo, Z.H., 1998. Late Paleozoic-Mesozoic intracontinental orogenic process and intermediate-acidic igneous rocks from the eastern Kunlun mountains of notrthwestern China. Geoscience 12, 344–352 (in Chinese with English abstract).

He, J.J., Ding, X., Wang, Y.R., Sun, W.D., Fu, B., 2015. The effect of temperature and concentration on hydrolysis of fluorine- rich titanium complexes in hydrothermal fluids: constraints on titanium mobility in deep geological processes. Acta Petrol. Sin. 31, 802–810 (in Chinese with English abstract).

Hu, Y., Niu, Y.L., Li, J.Y., Ye, L., Kong, J.J., Chen, S., Zhang, Y., Zhang, G.R., 2016. Petrogenesis and tectonic significance of the Late Triassic mafic dikes and felsic volcanic rocks in the East Kunlun Orogenic Belt, Northern Tibet Plateau. Lithos 245, 205–222.

Huang, H., Niu, Y.L., Nowell, G., Zhao, Z.D., Yu, X.H., Zhu, D.C., Mo, X.X., Ding, S., 2014. Geochemical constraints on the petrogenesis of granitoids in the East Kunlun Orogenic blet, northern Tibetan Plateau: implications for the continental crust growth through syncollisional felsic magmatism. Chem. Geol. 370, 1–18.

Huang, H., Niu, Y.L., Nowell, G., Zhao, Z.D., Yu, X.H., Mo, X.X., 2015. The nature and history of the Qilian Block in the context of the development of the Greater Tibetan Plateau. Gondwana Res. 28, 209–224.

Huang, H., Niu, Y.L., Mo, X.X., 2016. Syn-collisional granitoids in the Qilian Block on the Northern Tibetan Plateau: a long-lasting magmatism since continental collision through slab steepening. Lithos 246 (247), 99–109.

Hutchison, W., Pyle, D.M., Mather, T.A., Yirgu, G., Biggs, J., Cohen, B.E., Barfod, D.N., Lewi, E., 2016. The eruptive history and magmatic evolution of Aluto volcano: new insights into silicic peralkaline volcanism in the Ethiopian rift. J. Volcanol. Geoth. Res. 328, 9–33.

Jiang, C.F., Yang, J.S., Feng, B.G., Zhu, Z.Z., Zhao, M., Chai, Y.C., Shi, X.D., Wang, H.D., Hu, J.Q., 1992. Opening-closing tectonics of Kunlun Mountains. Ser. Geol. Memoirs 5, 1–224 (in Chinese with English abstract).

Kar, A., Weaver, B., Davidson, J., Colucci, M., 1998. Origin of differentiated volcanic and plutonic rocks from Ascension Island, South Atlantic Ocean. J. Petrol. 39, 1009–1024.

Keppler, H., 1993. Influence of fluorine on the enrichment of high field strength trace elements in granitic rocks. Contrib. Mineral. Petrol. 114, 479–488.

Kong, J.J., Niu, Y.L., Duan, M., Zhang, Y., Hu, Y., Li, J.Y., Chen, S., 2017. Petrogenesis of Luchuba and Wuchaba granitoids in western Qinling: geochronology and geochemical evidence. Mineral. Petrol 111, 887–908.

Kong, J.J., Niu, Y.L., Duan, M., Shao, F.L., Xiao, Y.Y., Zhang, Y., Guo, P.Y., Sun, P., Gong, H.M., 2019a. The syncollisional granitoid magmatism and crust growth during the West Qinling Orogeny, China: insights from the Jiaochangba pluton. Geol. J. 54, 4014–4033.

Kong, J.J., Niu, Y.L., Sun, P., Xiao, Y.Y., Guo, P.Y., Hong, D., Zhang, Y., Shao, F.L., Wang, X.H., Duan, M., 2019b. The origin and geodynamic significance of the Mesozoic dykes in eastern continental China. Lithos 332–333, 328–339.

Kong, J.J., Niu, Y.L., Hu, Y., Zhang, Y., Shao, F.L., 2020. Petrogenesis of the Triassic granitoids from the East Kunlun Orogenic Belt, NW China: implications for continental crust growth from syncollisional to post-collisional setting. Lithos 364-365, 105513. https://doi.org/10.1016/j.lithos.2020.105513.

Lee, C.T.A., Anderson, D.L., 2015. Continental crust formation at arcs, the arclogite "delamination" cycle, and one origin for fertile melting anomalies in the mantle. Sci. Bull. 60, 1141–1156.

Li, M., Zha, X.F., Hu, C.B., Gao, X.F., Li, T., Yao, Z.L., 2021. Zircon U-Pb geochronology of the Baishahe Formation in the western part of East Kunlun Orogenic Belt: constraints on Precambrian basement evolution. Geol. Bull. China 40, 41–57 (in Chinese with English abstract).

Li, R.B., Pei, X.Z., Li, Z.C., Liu, Z.Q., Chen, G.C., Chen, Y.X., Wei, F.H., Gao, J.M., Liu, C.J., Pei, L., 2012. Geological characteristics of Late Paleozoic-Mesozoic unconformities and their response to some significant tectonic events in eastern part of Eastern Kunlun. Earth Sci. Front. 19, 244–254 (in Chinese with English abstract).

Li, X.W., Huang, X.F., Luo, M.F., Dong, G.C., Mo, X.X., 2015a. Petrogenesis and geodynamic implications of the Mid-Triassic volcanic lavas from East Kunlun, northern Tibetan Plateau. J. Asian Earth Sci. 105, 32–47.

Li, X.W., Huang, X.F., Luo, M.F., Dong, G.C., Mo, X.X., 2015b. Petrogenesis and Geodynamic Implications of Middle and Late Triassic Volcanic Rocks in East Kunlun. Annual meeting of Chinese Geoscience Union, Beijing (in Chinese).

Li, X.W., Mo, X.X., Huang, X.F., Dong, G.C., Yu, X.H., Luo, M.F., Liu, Y.B., 2015c. U-Pb zircon geochronology, geochemical and Sr-Nd-Hf isotopic compositions of the Early Indosinian Tongren Pluton in West Qinling: Petrogenesis and geodynamic implications. J. Asian Earth Sci. 97, 38–50.

Li, Y.D., Liu, X.Y., 2014. Geochemical and tectonic setting of Late Triassic Volcanic rocks in Reshui area, Qinghai. Northwest Geol. 47, 14–25 (in Chinese with English abstract).

Li, Y.S., Xu, L.J., Yu, S.Y., Zhang, J.X., Guo, J., Peng, Y.B., Zhou, G.S., 2020. Partial melting of thickened lower crust in post-collisional setting: evidence from high silicon adakitic granites in the North Qilian orogen. Geol. J. 55, 3990–4007.
Liu, B., Ma, C.Q., Zhang, J.Y., Xiong, F.H., Huang, J., Jiang, H.A., 2013. Discovery of the Middle Devonian A-type granite from the Eastern Kunlun Orogen and its tectonic implications. Earth Sci J. China U. Geosci. 38, 947–962 (in Chinese with English abstract).
Liu, Q., Meng, F.C., Li, S.R., Feng, H.B., Jia, L.H., Tian, G.K., 2016. Geochronology of zircon from the paragneiss of Kuhai Group in southern East Kunlun terrane. Acta Petrol. Mineral. 35, 469–483 (in Chinese with English abstract).
Liu, Y., Gao, S., Hu, Z., Gao, C., Zong, K., Wang, D., 2010. Continental and oceanic crust recycling-induced melt- peridotite interactions in the trans-North China Orogen: U-Pb dating, Hf isotopes and trace elements in zircons from mantle xenoliths. J. Petrol. 51, 537–571.
Liu, Z.Q., Pei, X.Z., Li, R.B., Li, Z.C., Zhang, X.F., Liu, Z.G., Chen, G.C., Chen, Y.X., Ding, S. P., Guo, J.F., 2011. LA-ICP-MS zircon U-Pb dating of two suits of ophiolites at the Buqingshan area of the A'nyemaqen orogenic belt in the southern margin of the East Kunlun and its tectonic implication. Acta Geol. Sin. 85, 185–194 (in Chinese with English abstract).
Liu, Z., Jiang, Y.H., Jia, R.Y., Zhao, P., Zhou, Q., 2015. Origin of Late Triassic high-K calc-alkaline granitoids and their potassic microgranular enclaves from the western Tibet plateau, Northwest China: implications for Paleo-Tethys evolution. Gondwana Res. 27, 326–341.
Lowenstern, J.B., Mahood, G.A., 1991. New data on magmatic H_2O contents of pantellerites, with implications for petrogenesis and eruptive dynamics at Pantelleria. Bull. Volcanol. 54, 78–83.
Lu, W.Q., Tong, H.K., Cang, S.N.J.C., Ma, Y.S., 2012. Analysis of environment for Late Triassic volcanic rocks in Chachaxiangka. Elashan. Northwest Geol. 45, 48–55 (in Chinese with English abstract).
Ludwig, K., 2012. User's manual for isoplot version 3.75–4.15: a geochronological toolkit for microsoft. Excel Berkley Geochronol. Center Special Publ. 5, 1–75.
Luo, M.F., Mo, X.X., Yu, X.H., Li, X.W., Huang, X.F., Yu, J.C., 2014. Zircon LA-ICP-MS U-Pb dating, petrogenesis and tectonic implication of the Late Triassic granites from Xiangride area, East Kunlun. Acta Petrol. Sin. 30, 3229–3241 (in Chinese with English abstract).
Luo, Z.H., Ke, S., Cao, Y.Q., Deng, J.F., Shen, H.W., 2002. Late Indosinian mantle-derived magmatism in the East Kunlun. Geol. Bull. China 21, 291–297 (in Chinese with English abstract).
Ma, Z.Y., Ma, C.X., Ye, Z.F., Hao, Y., Ma, F.S., Tong, M.H., Zhou, Q.L., 2016. Rock and geochemical characteristics of late Triassic continental volcanic rock of Elashan group in the East Kunlun. J. Qinghai Univ. 34, 31–37 (in Chinese with English abstract).
Macdonald, R., Bagiński, B., Belkin, H.E., White, J.C., Noble, D.C., 2019. The Gold Flat Tuff, Nevada: Insights into the evolution of peralkaline silicic magmas. Lithos 328–329, 1–13.
Mahood, G., Hildreth, W., 1983. Large partition coefficients for trace elements in high-silica rhyolites. Geochim. Cosmochim. Ac. 47, 11–30.
Marks, M., Halama, R., Wenzel, T., Markl, G., 2004. Trace element variations in clinopyroxene and amphibole from alkaline to peralkaline syenites and granites: implications for mineral–melt trace-element partitioning. Chem. Geol. 211, 185–215.
Martin, R.F., 2006. A-type granites of crustal origin ultimately result from open-system fenitization-type reactions in an extensional environment. Lithos 91, 125–136.
Mbassa, B.J., Nionfang, E., Benoit, M., Kangang, P., Grégoire, M., Duchene, S., Brunet, P., Ateba, B., Tchoua, F.M., 2012. Mineralogy, geochemistry and petrogenesis of the recent magmatic formations from Mbengwi, a continental sector of the Cameroon Volcanic Line (CVL), Central Africa. Mineral. Petrol. 106, 217–242.
Meng, F.C., Cui, M.H., Wu, X.K., Wu, J.F., Wang, J.H., 2013. Magmatic and metamorphic events recorded in granitic gneisses from the Qimantag, East Kunlun Mountains, Northwest China. Acta Petrol. Sin. 29, 2107–2122 (in Chinese with English abstract).
Meng, F.C., Zhang, J.X., Yang, J.S., 2005. Tectono-thermal event of post-HP/UHP metamorphism in the Xitieshan area of the North Qaidam Mountains, western China: isotopic and geochemical evidence of Granite and gneiss. Acta Petrol. Sin. 21, 45–56 (in Chinese with English abstract).
Mo, X.X., Luo, Z.H., Deng, J.F., Yu, X.H., Liu, C.D., Shen, H.W., Yuan, W.M., Liu, Y.H., 2007. Granitoids and crust growth in the East-Kunlun Orogenic Belt. Geol. J. China Univ. 13, 403–414 (in Chinese with English abstract).
Mo, X.X., Niu, Y.L., Dong, G.C., Zhao, Z.D., Hou, Z.Q., Zhou, S., Ke, S., 2008. Contribution of syncollisional felsic magmatism to continental crust growth: a case study of the Paleocene Linzizong Volcanic Succession in southern Tibet. Chem. Geol. 250, 49–67.
Nash, W.P., Crecraft, H.R., 1985. Partition coefficients for trace elements in silicic magmas. Geochim. Cosmochim. Ac. 49, 2309–2322.
Ni, J., 2010. Zircon U-Pb age and tectonic setting of Permian-Triassic volcanic rocks in East Kunlun orogenic belt. M.S. thesis. Chinese Acad. Geol. Sci., Beijing 65 pp, (in Chinese with English abstract)..
Nishimura, K., 2012. A mathematical model of trace element and isotopic behavior during simultaneous assimilation and imperfect fractional crystallization. Contrib. Mineral. Petrol. 164, 427–440.
Niu, Y.L., Batiza, R., 1997. Extreme mantle source heterogeneities beneath the northern East Pacific Rise – Trace element evidence from near-ridge seamounts 15, 109–120.
Niu, Y.L., Collerson, K.D., Batiza, R., Wendt, J.I., Regelous, M., 1999. The origin of E-Type MORB at ridges far from mantle plumes: the East Pacific Rise at 11°20'N. J. Geophys. Res. 104, 7067–7087.
Niu, Y.L., O'Hara, M.J., 2003. Origin of ocean island basalts: A new perspective from petrology, geochemistry and mineral physics considerations. J. Geophys. Res. 108 (ECV 5), 1–19.
Niu, Y.L., O'Hara, M.J., 2009. MORB mantle hosts the missing Eu (Sr, Nb, Ta and Ti) in the continental crust: new perspectives on crustal growth, crust-mantle differentiation and chemical structure of oceanic upper mantle. Lithos 112, 1–17.
Niu, Y.L., Zhao, Z.D., Zhu, D.C., Mo, X.X., 2013. Continental collision zones are primary sites for net continental crust growth-A testable hypothesis. Earth-Sci. Rev. 127, 96–110.
Parker, D.F., Ren, M., Adams, D.T., Tsai, H., Long, L.E., 2012. Mid-Tertiary magmatism in western Big Bend National Park, Texas, U.S.A.: evolution of basaltic source regions and generation of peralkaline rhyolite. Lithos 144, 161–176.
Peccerillo, A., Barberio, M.R., Yirgu, G., Ayalew, D., Barbieri, M., Wu, T.W., 2003. Relationships between mafic and peralkaline silicic magmatism in continental rift settings: a petrological, geochemical and isotopic study of the Gedemsa volcano, central Ethiopian Rift. J. Petrol. 44, 2003–2032.
Peccerillo, A., Donati, C., Santo, A.P., Orlando, A., Yirgu, G., Ayalew, D., 2007. Petrogenesis of silicic peralkaline rocks in the Ethiopian rift: geochemical evidence and volcanology implications. J. Afr. Earth Sci. 48, 161–173.
Pidgeon, R.T., Nemchin, A.A., Hitchen, G.J., 1998. Internal structure of zircons from Archaean granites from the Darling Range batholith: implications for zircon stability and interpretation of zircon U-Pb ages. Contrib. Mineral. Petrol. 132, 288–299.
Qi, S., 2015. Petrotectonic assemblages and tectonic evolution of the East Kunlun orogenic belt in Qinghai Province. Ph.D. thesis, China University of Geosciences (Beijing), 334 pp (in Chinese with English abstract)..
Reiners, P.W., Nelson, B.K., Ghiorso, M.K., 1995. Assimilation of felsic crust by basaltic magma: Thermal limits and extents of crustal contamination of mantle-derived magmas. Geology 23, 563–566.
Ren, H.D., Wang, T., Zhang, L., Wang, X.X., Huang, H., Feng, C.Y., Teschner, C., Song, P., 2016. Ages, sources and tectonic settings of the triassic igneous rocks in the easternmost Segment of the East Kunlun Orogen, Central China. Acta Geol. Sin. (English Edition) 90, 641–668.
Renna, M.R., Tribuzio, R., Braga, R., 2013. Petrogenesis relationships between peralkaline rhyolite dykes and mafic rocks in the post-Variscan gabbroic complex from Bocca di Tenda (Northern Corsica, France). Contrib. Mineral. Petrol. 165, 1073–1085.
Rollinson, H., 1993. Using Geochemical Data: Evaluation, Interpretation, Presentation. Longman Scientific and Technical xxvi. Wiley, p. 352.
Rubatto, D., Gebauer, D., 2000. Use of cathodoluminescence for U-Pb zircon dating by IOM Microprobe: Some examples from the western Alps. In: Pagel, M., Barbin, V., Blanc, P. (Eds.), Cathodoluminescence in Geoscience. Springer-Verlag, Berlin Herdelberg, Germany, pp. 373–400.
Rudnick, R.L., Gao, S., 2003. Composition of the continental crust. In: Holland, H.D., Turekian, K.K. (Eds.), Treatise on Geochemistry 3. Elsevier-Pergamon, Oxford, pp. 1–64.
Sacks, P.E., Secor, D.T., 1990. Delamination in collisional orogens. Geology 18, 999–1002.
Shao, F.L., Niu, Y.L., Liu, Y., Chen, S., Kong, J.J., Duan, M., 2017. Petrogenesis of Triassic granitoids in the East Kunlun Orogenic Belt, northern Tibetan Plateau and their tectonic implications. Lithos 282 (283), 33–44.
Shao, F.L., Niu, Y.L., Marcel, R., Zhu, D.C., 2015. Petrogenesis of peralkaline rhyoliths in an intro-plate setting: Glass House Mountains, southeast Queensland, Australia. Lithos 216 (217), 196–210.
Song, S.G., Niu, Y.L., Su, L., Xia, X.H., 2013. Tectonics of the North Qilian orogen. NW China. Gondwana Res. 23, 1378–1401.
Sun, P., Niu, Y.L., Guo, P.Y., Cui, H.X., Ye, L., Liu, J.J., 2018. The evolution and ascent paths of mantle xenolith-bearing magma: observations and insights from Cenozoic basalts in Southeast China. Lithos 310–311, 171–181.
Sui, Q.L., Wang, Q., Zhu, D.C., Zhao, Z.D., Chen, Y., Santosh, M., Hu, Z.C., Yuan, H.L., Mo, X.X., 2013. Compositional diversity of ca. 110 magmatism in the northern Lhasa Terrane, Tibet: implications for the magmatic origin and crustal growth in a continent–continent collision zone. Lithos 168–169, 144–159.
Sun, Y., 2004. Gonghe aulacogen and conjugate and transfer between the west Qinling and east Kunlun orogen. Ph.D. thesis, Northwest University, Xi'an. 206 pp (in Chinese with English abstract).
Sun, W.D., McDonough, W.F., 1989. Chemical and isotopic systematics of oceanic basalts: implications for mantle composition and processes. Geol. Soc. London Special Publ. 42, 313–345.
Tong, H.K., Wang, S.L., Song, S.C., Tan, S.X., Ma, X.L., Huang, Q.H., 2004. Study on volcanic rocks and their structural environment of Late Triassic epoch in Chachaxiangka area in Qinghai Province. Plateau Earthquake Res. 16, 38–48 (in Chinese with English abstract).
Vavra, G., Gebauer, D., Schmid, R., Compston, W., 1996. Multiple zircon growth and recrystallization during polyphase Late Carboniferous to Triassic metamorphism in granulites of the Ivrea Zone (South Alps): An ion microprobe (SHRIMP) study. Contrib. Mineral. Petrol. 122, 337–358.
Wang, B.D., Wang, L.Q., Wang, D.B., Yin, F.G., He, J., Peng, Z.M., Yan, G.C., 2018. Tectonic Evolution of the Changning-Menglian Proto-Paleo Tethys Ocean in the Sanjiang Area, Southwestern China. Earth Sci. 43, 2527–2550 (in Chinese with English abstract).

Wang, K.X., Yu, C.D., Yan, J., Liu, X.D., Liu, W.H., Pan, J.Y., 2019. Petrogenesis of Early Silurian granitoids in the Longshoushan area and their implications for the extensional environment of the North Qilian Orogenic Belt, China. Lithos 342–343, 152–174.

Watson, E.B., Harrison, T.M., 1983. Zircon saturation revisited: temperature and composition effects in a variety of crustal magma types. Earth Planet. Sci. Lett. 64, 295–304.

White, J.C., Espejel-Garcia, V.V., Anthony, E.Y., Omenda, P., 2012. Open system evolution of peralkaline trachyte and phonelite from the Suswa volcano, Kenya rift. Lithos 152, 84–104.

Wu, Y.B., Zheng, Y.F., 2004. Genetic mineralogy of zircon and its constraints on U-Pb age interpretation. Chin. Sci. Bull. 49, 1589–1604.

Xia, R., Wang, C.M., Deng, J., Carrancz, E.J.M., Li, W.L., Qing, M., 2014. Crustal thickening prior to 220 Ma in the East Kunlun Orogenic Belt: Insights from the Late Triassic granitoids in the Xiao-Nuomuhong pluton. J. Asian Earth Sci. 93, 193–210.

Xia, R., Wang, C.M., Qing, M., Li, W.L., Carranza, E.J.M., Guo, X.D., Ge, L.S., Zeng, G.Z., 2015. Zircon U-Pb dating, geochemistry and Sr–Nd–Pb–Hf–O isotopes for the Nan'getan granodiorites and mafic microgranular enclaves in the East Kunlun Orogen: record of closure of the Paleo-Tethys. Lithos 234–235, 47–60.

Xiao, Y.Y., Chen, S., Niu, Y.L., Wang, X.H., Xue, Q.Q., Wang, G.D., Gao, Y.J., Gong, H.M., Kong, J.J., Shao, F.L., Sun, P., Duan, M., Hong, D., Wang, D., 2020. Mineral compositions of syn-collisional granitoids and their implications for the formation of juvenile continental crust and adakitic magmatism. J. Petrol. 61 (3), egaa038. https://doi.org/10.1093/petrology/egaa038.

Xiong, F.H., Ma, C.Q., Zhang, J.Y., Liu, B., Jiang, H.A., 2014. Reworking of old continental lithosphere: an important crustal evolution mechanism in orogenic belts, as evidenced by Triassic I-type granitoids in the East Kunlun orogen, Northern Tibetan Plateau. J. Geol. Soc. 171, 847–863.

Xu, B., Li, H.B., Nan, Y.Y., Wang, C.Y., Yue, T., Zhao, M.F., 2019. LA-MC-ICP-MS Zircon U-Pb ages, geochemical characteristics and tectonic significance of the Late Triassic igneous rocks in Ageteng area, Qimantage Mountains. Geol. Rev. 65, 353–369 (in Chinese with English abstract).

Xu, B., Li, Y.L., Shi, L.C., Zhang, H.Q., Ma, D.Q., Ren, X., Wang, C.Y., 2020a. Magmatic consanguinity of the Late Triassic granites and rhyolites in eastern Qimantage: Constraints from geochronology, geochemistry and Nd-Pb isotopes. Geol. Rev. 66, 686–698 (in Chinese with English abstract).

Xu, J.F., Castillo, P.R., 2004. Geochemical and Nd–Pb isotopic characteristics of the Tethyan asthenosphere: implications for the origin of the Indian Ocean mantle domain. Tectonophysics 393, 9–27.

Xu, X., Liu, C.F., Liu, W.C., Ye, B.Y., Zhao, Z.D., Ma, B., 2020b. Geochronology and geochemistry of the Late Devonian-Early Carboniferous volcanic rocks in Aksu River area, western end of the East Kunlun Orogen. Geol. J. 55, 2881–2901 (in Chinese with English abstract).

Xu, Z.Q., Yang, J.S., Li, H.B., Zhang, J.X., Wu, C.L., 2007. Orogenic Plateau: Terrane Amalgamation, Collision and Uplift in the Qinghai-Tibet Plateau. Geological Publishing House, Beijing. , 458 pp (in Chinese).

Xu, Z.Q., Yang, J.S., Li, W.C., Li, H.Q., Cai, Z.H., Yan, Z., Ma, C.Q., 2013. Paleo-Tethys system and accretionary orogen in the Tibet Plateau. Acta Petrol. Sin. 29, 1847–1860 (in Chinese with English abstract).

Yan, Z., Bian, Q.T., Korchagin, O.A., Pospelov, I.I., Li, J.L., Wang, Z.Q., 2008. Provenance of Early Triassic Hongshuichuan formation in the southern margin of the East Kunlun Mountains: constrains from detrial framework, heavy mineral analysis and geochem istry. Acta Petrol. Sin. 24, 1068–1078 (in Chinese with English abstract).

Yang, J.S., Robinson, P.T., Jiang, C.F., Xu, Z.Q., 1996. Ophiolites of the Kunlun mountains, China and their tectonic implications. Tectonophysics 258, 215–231.

Yang, J.S., Shi, R., Wu, C.F., Wang, X.B., 2009. Dur'ngio ophiolite in east Kunlun, northeast Tibetan plateau: evidence for Paleo-Tethyan suture in northwest China. J. Earth Sci. 20, 303–331.

Yin, H.F., Zhang, K.X., 1998. Evolution and characteristics of the central orogenic belt. Earth Sci. J. China U. Geosci. 23, 438–442 (in Chinese with English abstract).

Zhang, S.Q., Wang, J., Wang, B.Z., Zhuang, Y.C., 2000. Study on the orogenic mechanism of the Elashan intracontinental oblique thrust magmatic orogenic belt in the joint of Kunlun and Qinling. Collection of important achievements of Ninth Five-Year Plan in geological science and technology, pp. 80–85 (in Chinese)..

Zhao, X., Wei, J.H., Fu, L.B., Huizenga, J.M., Santosh, M., Chen, J.J., Wang, D.Z., Li, A.B., 2020. Multi-stage crustal melting from Late Permian back-arc extension through Middle Triassic continental collision to Late Triassic post-collisional extension in the East Kunlun Orogen. Lithos 360–361, 105446. https://doi.org/10.1016/j.lithos.2020.105446.